

## FINAL REPORT

---

# ADAPTING THE SAPRC CHEMISTRY MECHANISM FOR LOW TEMPERATURE CONDITIONS

### Submitted to:

**Patrick Barickman, Manager and Technical Analysis**

Utah Division of Air Quality

195 N 1950 W, Salt Lake City, UT 84114

### Submitted by:

**Marc Mansfield, Senior Environmental Modeler**

Bingham Entrepreneurship & Energy Research Center

Utah State University, Vernal, Utah

**Jaron C. Hansen, Professor**

Chemistry and Biochemistry Department

Brigham Young University, Provo, Utah

### Authors:

**Huy Tran, PhD**

**Marc Mansfield, PhD**

**Trang Tran, PhD**

Bingham Entrepreneurship & Energy Research Center

Utah State University, Vernal, Utah

**Sambhav Kumbhani, PhD**

**Jaron C. Hansen, PhD**

Chemistry and Biochemistry Department

Brigham Young University, Provo, Utah

**DOCUMENT NUMBER:** BRC\_NNNNN  
**REVISION:** ORIGINAL RELEASE  
**DATE:** SEPTEMBER 30, 2015



## Contents

---

EXECUTIVE SUMMARY .....	3
1. INTRODUCTION.....	4
2. ANALYTICAL METHOD .....	5
3. MODELING EPISODES AND SENSITIVITY SIMULATIONS.....	18
4. MODEL PERFORMANCE.....	19
5. RESULTS AND DISCUSSIONS.....	22
6. CONCLUSIONS AND RECOMMENDATIONS .....	28
7. REFERENCES.....	30

## EXECUTIVE SUMMARY

---

In this study, the Statewide Air Pollution Research Center 2007 (SAPRC07) model chemical mechanism has been modified to adapt to low temperature conditions for simulating high ozone ( $O_3$ ) episodes during winter in the Uintah Basin, Utah. A model chemical mechanism describes the chemical reactions of numerous gaseous species to be simulated by photochemical models. SAPRC07 and other widely used mechanisms, such as the Carbon Bond 2005 (CB05), have been primarily developed and tested for tropospheric  $O_3$  pollution in urban areas during summertime and it has been unclear whether they faithfully represent the low-temperature, low-humidity conditions of the winter ozone phenomenon. This presents the need of adapting the SAPRC07 mechanism to low winter conditions because: (1) some chemical reactions that are not important under summer and urban conditions become important under winter and oil and gas emission; (2) model chemical mechanisms are not frequently updated with up-to-date new measurements of chemical reactions.

We have performed a literature search of a number of important chemical reactions, identifying the most up-to-date measurements of their low-temperature, low-humidity behavior. These results have been imported into the SAPRC07 mechanism. These updates include modifications made to five photolysis and 40 non-photolysis reactions, and introducing of new chemical species. The most outstanding modifications are the introduction to SAPRC07 of a low-temperature nitric acid ( $HNO_3$ ) branching effect and of methane ( $CH_4$ ) reactions that potentially are important for  $O_3$  formation under low temperature and low humidity conditions in the Uintah Basin. The improvements were incorporated into the Community Multi-scale Air Quality (CMAQ) photochemical model at source-code level.

We evaluate the effects of improvements made to SAPRC07 mechanism on winter  $O_3$  formation by examining outputs of different sensitivity simulations performed with the Community Multi-scale Air Quality (CMAQ) model. The net effects of the introduction of the  $HNO_3$  branching effect and of the  $CH_4$  chemistry are to decrease and increase  $O_3$  formation, respectively, which are consistent with literature reviews. When all updates are applied to Uintah Basin models, the predictions for ozone decrease somewhat. However, we believe that current estimates of emissions into the atmosphere are too low, and that corrections to these will compensate for the lower predictions.

Based on the outcome of this project, we propose these recommendations:

1. Methane chemistry has proved to be important for  $O_3$  formation in the Uintah Basin under winter conditions and with emissions from oil and gas industry. We suggest that methane chemistry should be considered in all model mechanisms for adequate simulation of winter  $O_3$  in the Basin.
2. Improvements in emission inventory (EI) are critical for better  $O_3$  simulation performance. Especially, improvement on  $CH_4$  emissions are necessary as current  $CH_4$  emissions led to high under-estimation of  $CH_4$  concentrations. EI improvements should also include more representative VOC speciation profiles for emissions from oil and gas industry.
3. Effects of modifications made to SPARC07 should be re-evaluated with the improved emission inventory.

## 1. INTRODUCTION

---

Elevated ozone ( $O_3$ ) levels have occurred in the Uintah Basin during the recent past winters (Figure 1.1). Ozone is identified by the Environmental Protection Agency (EPA) as a criteria pollutant, and under the requirements of the Clean Air Act, Duchesne and Uintah counties are likely to enter non-attainment for ozone. Non-attainment status implies that state and local governments will be required to plan and implement strategies for ozone abatement. The chemical mechanism driving  $O_3$  formation is well understood in general: it is the product of photolysis and non-photolysis reactions of nitrogen oxides ( $NO_x$ , comprised of NO and  $NO_2$ ) and volatile organic compounds (VOCs) under influences of short-wave solar radiation. However, such reactions occur in various ways depending on local atmospheric composition and meteorology. Elevated  $O_3$  commonly occurs in populated urban areas (e.g., Los Angeles, Sacramento) with high- $NO_x$ -to-VOCs emissions and in summer when solar radiation is most intense and temperature is high ( $>300$  K). The winter ozone phenomenon in the Uintah Basin is unique as it occurred during the time when both incoming solar radiation and temperature are at the lowest in a year ( $300 - 600$  W/m<sup>2</sup>,  $260 - 270$  K) and with high oil and gas activities. Control strategies that would be advisable in, say, the Los Angeles Basin could very well be counterproductive in the Uintah Basin.

Photochemical models have been widely employed as scientific as well as regulatory tools for studying elevated  $O_3$  events. Acting at the heart of photochemical models are chemical mechanisms that direct the models in simulating chemical reactions in the atmosphere. The Carbon Bond 2005, CB05 (Yarwood et al. 2005); the Regional Atmospheric Chemistry Mechanism version 2, RACM2 (Goliff et al. 2013); and the Statewide Air Pollution Research Center-2007, SAPRC07 (Carter 2010) are chemical mechanisms that are most widely employed in photochemical models. These mechanisms are based on smog chamber experiments and have been primarily developed and tested for tropospheric ozone pollution in urban areas during summer time. While examining these chemical mechanisms for their applicability for winter  $O_3$  simulation, we have identified several discrepancies:

- (i) Ozone pollution in the Uintah Basin, UT commonly occurs in wintertime when temperatures range between  $260-270$  K. Meanwhile, chemical mechanisms were typically developed for studying ozone pollution in urban areas during summertime at a reference temperature of  $300$  K. Chemical reactions are known to behave differently at different temperatures. For example, in the SPARC07 mechanism most non-aromatic VOCs are parameterized at  $300$  K (Carter and Seinfeld 2012). Carter and Seinfeld (2012) developed a specific version of SAPRC07 for a box model in which non-aromatic VOC reaction rates were derived at  $265$  K to examine ozone formation in the Upper Green River Basin. These adjustments produced a decrease in  $NO$  to  $NO_2$  conversions, and an increase in overall nitrate formation. This plays as the termination on the  $NO_x$  reaction chain which leads to  $O_3$  formation reduction. Based on the field campaign performed in Uintah Basin in winter 2012, Lee et al. (2014) estimated that alkyl nitrate formation, as the product of reactions between VOCs and  $NO_x$ , were enhanced by 30% which led to a suppression of  $O_3$  formation by 20% as temperature decreased from  $300$  to  $273$  K. Such substantial temperature dependent effects should be considered in the model chemical mechanism (Lee et al. 2014). The effect of organic nitrate formation enhancement under low temperature conditions had been included in the Carbon Bond 2006 (CB06) chemical mechanism and examined using the CAMx model which showed a decrease in winter  $O_3$  formation in the Uintah Basin (Emery and Yarwood 2015).
- (ii) Many chemical reactions that are negligible under summertime conditions become important for ozone formation under wintertime conditions. For example, Butkovskaya et al. (2005) reported that formation of nitric acid ( $HNO_3$ ) from the reaction between hydroxyl peroxide ( $HO_2$ ) and  $NO$  increased five-fold as the temperature decreased from  $298$  to  $223$  K. The formation of  $HNO_3$  suppresses  $HO_2$  and  $NO$  cycles which

would lead to reduction in O<sub>3</sub> formation. Our justifications also showed that under dry conditions and with high methane (CH<sub>4</sub>) concentration emitted from the oil and gas industry and trapped under a strong inversion layer during winter in Uintah Basin, chemical reactions involving CH<sub>4</sub> chemistry become important for O<sub>3</sub> formation. Details on HNO<sub>3</sub> formation and CH<sub>4</sub> chemistry will be discussed further in Section 2.1.2. To our best knowledge, such reactions have not been considered in the latest chemical mechanisms.

(iii) New measurements on chemical reactions have become available over time but not all of them have been incorporated into the chemical mechanisms. New chemical reaction measurements are often reviewed and elected for recommended values by the International Union of Pure and Applied Chemistry (IUPAC 2015) as frequent as monthly. The NASA Jet Propulsion Laboratory (Sander et al. 2011) publishes its reviews and suggested chemical kinetics and photochemical data in every two or three years. Meanwhile new versions of photochemical models, such as the Community Multi-scale Air Quality (CMAQ; Byun and Schere 2006), are released every two or three years with little to no updates of the chemical mechanisms. Therefore, the chemical mechanisms are not incorporated with the most up-to-date chemical reaction values of which many are temperature dependent.

The above discrepancies raise a critical need for improving chemical mechanisms to account for the fundamental differences between winter and summer ozone. In this study, we implemented modifications to the SAPRC07 chemical mechanism to adapt it to low temperature conditions for simulating elevated winter O<sub>3</sub> even in the Uintah Basin. The SAPRC07 is one of three chemical mechanisms that have been incorporated into the CMAQ photochemical grid model. SAPRC07 is more chemically detailed than CB05, and therefore is usually more computationally expensive. However, it is still a good candidate for studying winter ozone pollution in the Uintah Basin where chemical accuracy is a priority. SAPRC07 was used in a box model study of winter ozone in the Upper Green River Basin of Wyoming [Carter and Seinfeld, 2012] but has not been applied in winter ozone studies using a comprehensive air quality model like CMAQ.

## 2. ANALYTICAL METHOD

---

### 2.1. SAPRC07 modifications

#### 2.1.1. Photolysis reactions

Out of the total of 39 photolysis reactions considered in SAPRC07, we made modifications to four reactions including: NO<sub>2</sub>, ozone atoms (O<sup>1</sup>D and O<sup>3</sup>P), formaldehyde (HCHO), and nitric acid (HNO<sub>3</sub>). Modifications made to SAPRC07 include updates in actinic flux, quantum yield and absorption cross sections, and improvement in temperature and pressure dependence of quantities. Details on modification made to each of the four photolysis reactions are described in the subsequent sections.

For a better understanding, one should understand how the SAPRC07 mechanism parameterizes photolysis reactions: the photolysis reaction rate  $J$  (1/s) can be expressed as:

$$J = \int_{\lambda_1}^{\lambda_2} \sigma(\lambda, T) \phi(\lambda, T) I(\lambda) d\lambda$$

where  $\lambda_1$  and  $\lambda_2$  are lower and upper limits of a wavelength bin (nm),  $T$  is the atmospheric temperature (K),  $\sigma$  is the absorption cross-section (cm<sup>2</sup>),  $\phi$  is the quantum yield (1/photon), and  $I$  is actinic flux (photon/cm<sup>2</sup>.nm.s). Currently SAPRC07 considers wavelengths ranging from 291 – 850 nm which are divided into seven wavelength-bins following a fast-J photolysis scheme (Wild et al. 2000). Furthermore, SAPRC07 considers temperatures ranging from 210 – 310 K which are divided into six temperature bins of 20 K intervals. Values of  $\sigma$  and  $\phi$  are pre-calculated for seven wavelength and six temperature bins for each of the 39 photolysis reactions. Values of  $\sigma$  and  $\phi$  for specific  $\lambda$  and  $T$  are linearly interpolated from

lower and upper wavelength and temperature limits of the bins that they fall into. Additional steps of  $\sigma$  and  $\phi$  corrections for their dependences on pressure and other driving factors are handled by the photolysis module (PHOT\_MOD.F) of CMAQ model.

## NO<sub>2</sub>

The photolysis reaction of NO<sub>2</sub> is expressed as:



We calculated  $\sigma$  at temperatures of 223, 246, 260, 280 and 293K and for wavelengths from 290 – 800 nm in 0.01 nm increment based on data published by Voigt et al. (2002). After that, we applied a solar-flux-intensity weighting factor to the averaging of  $\sigma$  for seven wavelength bins. Finally, we developed second-order fitting equation for the averaged- $\sigma$  to extrapolate  $\sigma$  to 11 temperature bins ranging from 210 – 310K in 10K increment. This means we refined the temperature bins from the original six bins in order to better represent the non-linear temperature dependence of  $\sigma$ . The above treatments improved temperature dependent of  $\sigma$  and kept the modifications compatible with fortran subroutines of the CMAQ photolysis module. No improvement was made to  $\phi$  as no update value was found. The net effect of these modifications is an increase in  $\sigma$  that eventually led to an increase in NO<sub>2</sub> photolysis rate. Additionally, the updated  $\sigma$  becomes positive temperature-dependent as opposed to the slight negative temperature-dependence of the unmodified  $\sigma$ .

## O<sub>3</sub> (O<sup>1</sup>D and O<sup>3</sup>P)

The photolysis reaction of O<sub>3</sub> is expressed as:



We updated  $\sigma_{R2}$  and  $\sigma_{R3}$  with the high spectral resolution ozone absorption cross-section published by Serdyuchenko et al. (2013) and with the high solar reference spectrum for earth's atmosphere (Chance and Kurucz 2010). As in treatments for NO<sub>2</sub>,  $\sigma_{R2}$  and  $\sigma_{R3}$  were averaged for seven wavelength and 11 temperature bins using solar-flux-intensity weighting factor and second-order fitting equation.

Both IUPAC (2015) and Sander et al. (2011) recommend temperature dependence of  $\phi$  for O<sup>1</sup>D production from O<sub>3</sub> photolysis reactions for 306 <  $\lambda$  < 328 nm and 200 < T < 320 K as follows:

$$\phi_{R2}(\lambda, T) = \left\{ \frac{q_1}{q_1 + q_2} \right\} \times A_1 \times \exp \left\{ - \left( \frac{X_1 - \lambda}{\omega_1} \right)^4 \right\} + \left\{ \frac{q_2}{q_1 + q_2} \right\} \times A_2 \times \left\{ \frac{T}{300} \right\}^2 \exp \left\{ - \left( \frac{X_2 - \lambda}{\omega_2} \right)^2 \right\} + A_3 \times \left\{ \frac{T}{300} \right\}^{1.5} \exp \left\{ - \left( \frac{X_3 - \lambda}{\omega_3} \right)^2 \right\} + c \quad (1)$$

where

$$q_i = \exp \left( - \frac{v_i}{RT} \right)$$

$$A_1 = 0.8036; A_2 = 8.9061; A_3 = 0.1192; X_1 = 304.225; X_2 = 314.957; X_3 = 310.737;$$

$$\omega_1 = 5.576; \omega_2 = 6.601; \omega_3 = 2.187; v_1 = 0; v_2 = 825.518; c = 0.0765$$

and

$$\phi_{R2} = 1 - \phi_{R3}$$

Due to the strong non-linear temperature-dependence of  $\phi_{R2}$  as shown in Eq. (1), instead of calculating tabulated values for the corresponding wavelength and temperature bins, we implemented Eq. (1) into the source-code of CMAQ photolysis module. We applied the original SAPRC07 values of  $\phi$  for  $\lambda$  values outside the applicable ranges of Eq. (1).

### HCHO (HCHOR and HCHOM)

The photolysis reaction of HCHO is expressed as:



Note that reactions (R4) and (R5) are represented as photolysis reactions HCHOR and HCHOM in the SAPRC07 mechanism.

We updated  $\sigma$  values for HCHO for  $290 < \lambda < 348$  nm and  $223 < T < 323$  K using the recommended relationship (Sander et al. 2011; IUPAC 2015):

$$\sigma(\lambda, T) = \sigma(\lambda, 298 \text{ K}) + \Gamma(\lambda)(T - 298 \text{ K}) \quad (2)$$

where the wavelength-dependent factor  $\Gamma(\lambda)$  is provided. The  $\sigma(\lambda, T)$  values derived from Eq. (2) were then averaged for corresponding wavelength and temperature bins. For  $\lambda$  and  $T$  outside the applicable ranges of Eq. (2), their  $\sigma$  values were assigned with original SAPRC07 values of the bins into which they fall.

IUPAC (2015) suggests that for  $306 < \lambda < 328$  nm, both  $\phi_{R4}$  and  $\phi_{R5}$  are independent of temperature and pressure; for  $330 < \lambda < 360$  nm,  $\phi_{R5}$  is subject to Stern-Volmer pressure quenching:

$$\frac{1}{\phi_{R5}} = 1 + \frac{k_q}{k_d} \times [M] \quad (3)$$

where  $k_q/k_d$  is the quenching coefficient ( $1/\text{cm}^3 \cdot \text{molecule}$ ) which increases with decreasing temperature and wavelength;  $[M]$  is the concentration of air molecules. Values for  $k_q/k_d$  are provided for wavelengths at 329 and 353 nm and temperatures at 399 and 220 K. Using a linear interpolation approach, we determined  $k_q/k_d$  for other wavelength intervals within 330 – 360 nm and applied Eq. (3) to determine  $\phi_{R5}$  for the corresponding wavelength bins (bin 5 and 6). Note that we implemented Eq. (3) into the source-code of the CMAQ photolysis module.

### HNO<sub>3</sub>

The photolysis reaction of HNO<sub>3</sub> is expressed as:



Sander et al. (2011) recommends that for  $192 < \lambda < 350$  nm,  $\sigma_{R6}$  is temperature dependent following Burkholder et al. (1993)'s relationship:

$$\sigma(\lambda, T) = \sigma(\lambda, 298 \text{ K}) \exp(B(\lambda)(T - 298)) \quad (4)$$

where the  $B(\lambda)$  coefficient value is provided. Instead of calculated tabulated  $\sigma_{R6}$  values for the corresponding wavelength and temperature bins, we implemented Eq. (4) into the source-code of the CMAQ photolysis module for better temperature-dependent characterization of  $\sigma_{R6}$ .

Table 2.1 summaries modifications that we implemented to the photolysis reactions in SAPRC07 mechanism.

**Table 2.1.** Updates made to photolysis reactions in SAPRC07T mechanism and their references

ID	Before Updating		After updating	
	Cross section	Quantum yield	Cross section	Quantum yield
NO <sub>2</sub>	Sander et al. 2006	Sander et al. 2006	Voigt et al. 2002	Sander et al. 2006 <sup>a</sup>
O <sub>3</sub>	Sander et al. 2006	Sander et al. 2006	Serdyuchenko et al. 2013	Sander et al. 2006 <sup>b</sup>
HCHO	Sander et al. 2006	Sander et al. 2006	Sander et al. 2011	IUPAC 2015
HNO <sub>3</sub>	Sander et al. 2006	Sander et al. 2006	Sander et al. 2011 <sup>c</sup>	Sander et al. 2011

<sup>a</sup> Linearly interpolated from six temperature bins to 11 temperature bins

<sup>b</sup> Temperature and wavelength dependences of O<sup>1</sup>D quantum yield within 306 – 328 nm wavelength were implemented in CMAQ photolysis module at source-code level instead of using tabulated data.

<sup>c</sup> Same values were recommended in Sander et al. 2006 and 2011. However, temperature dependence of the absorption cross section for wavelengths 192-350 nm is implemented into CMAQ source in this study.

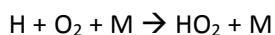
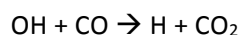
### 2.1.2. Non-photolysis reactions

Overall, we updated 40 reactions based on updated recommendations from IUPAC (2015), Sander et al. (2011) and other peer-reviewed articles. The updates include 11 new reactions to describe a nitric acid (HNO<sub>3</sub>) branching effect and methane (CH<sub>4</sub>) chemistry that are expected to be important for ozone formation under winter condition in the Basin. Additionally, we carried over many updates made to the SAPRC11 mechanism (Carter and Heo 2013) to the SAPRC07. Note that several aromatic organic compound related reactions in SAPRC07 had been updated in SAPRC11 which have not been supported in the current versions of photochemical models.

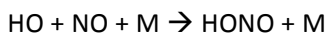
Justifications for the modifications to the HNO<sub>3</sub> branching effect and to CH<sub>4</sub> chemistry are discussed in the subsequent sections. Table 2.2 summarizes other modifications made to the SAPRC07 non-photolysis reactions, and Table 2.3 summarizes updates from SAPRC11 that had been implemented in SAPRC07.

#### **HNO<sub>3</sub> branching effect**

The conversion of NO to NO<sub>2</sub> by reacting with hydroxyl peroxide radical (HO<sub>2</sub>) primarily occurs in the following pathway (e.g., Mihele et al. 1999, Coll et al. 2005):



The chain reaction is mainly terminated by the formation of HONO:



Reichert et al. (2003) showed evidence that formation of HNO<sub>3</sub> via the following HO<sub>2</sub> + NO reaction also contributes to the termination of reaction (R7):



The rate constants of reactions (R7) and (R8) at 298 K are  $8.8 \times 10^{-12}$  and  $1.6 \times 10^{-14}$ , respectively.

A detail studied conducted by Butkovskaya et al. (2005) showed that HNO<sub>3</sub> formation from reaction (R8) is relatively small under room temperature conditions but increases significantly as temperature decreases. More specifically, the product branching ratio (R8)/(R7) increased by nearly 5-fold as the temperature decreased from 298K to 223K (Figure 2.1). The branching ratio further increases under the presence of water vapor.

Similar to the enhancement of alkyl nitrate formation (Lee et al. 2014), the enhancement of HNO<sub>3</sub>

formation under low temperature conditions is also an important termination of  $\text{NO}_x$  and  $\text{HO}_x$ , and thus is important to  $\text{O}_3$  formation. Since reaction (R8) has not been considered in any chemical mechanism, it is tempting to implement this low temperature effect into the SAPRC07 mechanism and examine its impact on  $\text{O}_3$  and other species. Reaction (R8) is included in SAPRC07 and is presented as reactions <LT01> in Table 2.2. The effect of water vapor on reaction (R8) is treated analogously to the effect of water vapor on the reaction of  $\text{HO}_2 + \text{HO}_2 \rightarrow \text{H}_2\text{O}_2 + \text{O}_2$  (Kircher and Sander 1984) and is presented by reaction <LT02>.

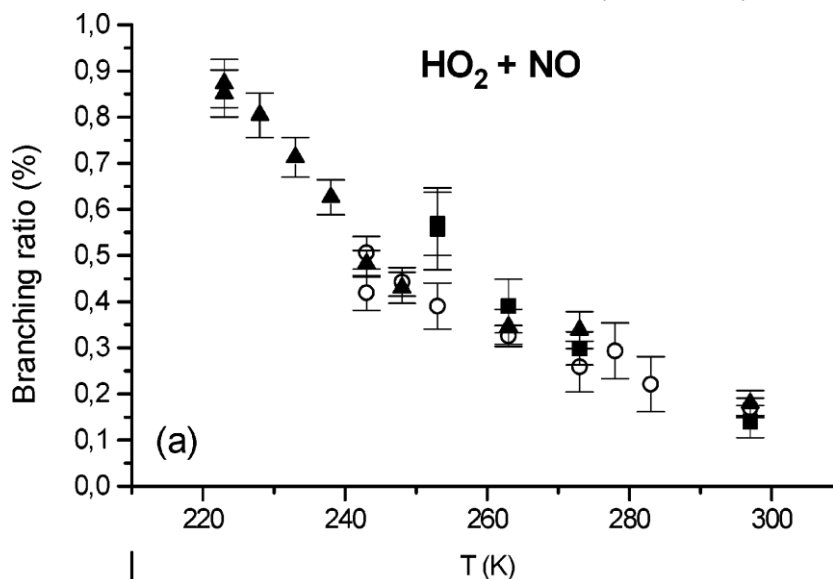


**Figure 2.1.** Temperature dependence of the branching ratio of the  $\text{HNO}_3$  formation of the  $\text{HO}_2 + \text{NO}$  reaction. Symbols of triangles, squares and circles represent measurements obtained from various experiments. (Ref: Figure 8(a) by Butkovskaya et al. 2005)

#### ***CH<sub>4</sub> chemistry***

Almost all ozone atom  $\text{O}^1\text{D}$  is consumed by its reaction with water vapor to form OH radical (Sander et al. 2011):



with rate constant  $k(T) = 1.63 \times 10^{-10} \times \exp(60/T)$  and  $k(298\text{K}) = 2.0 \times 10^{-10}$

$\text{O}^1\text{D}$  also converts to  $\text{O}^3\text{P}$  at a much slower rate ( $k(298\text{K}) = 3.1 \times 10^{-11}$ ):



Furthermore,  $\text{O}^1\text{D}$  reacts with  $\text{CH}_4$  in chain reactions (IUPAC 2015, Schocker et al. 2007):



The rate constants of reactions (R10) through (R13) at 298K are  $1.05 \times 10^{-10}$ ,  $7.5 \times 10^{-12}$ ,  $3.45 \times 10^{-11}$ , and  $9.4 \times 10^{-12}$ . The rate constant of reaction (R10) indicates that this reaction occurs half as fast as reaction (R9). However, water vapor is abundant in the atmosphere: water mixing ratio at 35° latitude and in July is approximately  $14 \times 10^3$  ppm near the surface and  $10^3$  ppm at about 7 km above sea level (Sun and Lindzen 1993). Meanwhile, the tropospheric background  $\text{CH}_4$  concentration is approximately 1.9 ppm (Blasing 2015). Because of the domination of water vapor over  $\text{CH}_4$ , most  $\text{O}^1\text{D}$  is consumed by reaction (R9). Since the chemical mechanisms are typically developed for summer ozone phenomenon and for mid-to-low latitude regions, it is understandable that reactions (R10) through (R13) are not considered in these mechanisms.

Justifications exist for the importance of reactions (R10) through (R13) on O<sub>3</sub> chemistry during winter in the Uintah Basin. Firstly, there is less water vapor in winter than in summer: at 35° latitude in January, water vapor decreases to 6 x 10<sup>3</sup> ppm at near surface layer and 0.5 x 10<sup>3</sup> ppm at about 7 km above sea level (Sun and Lindzen 1993). Our meteorological model estimated water vapor at 10<sup>3</sup> ppm in January in the Uintah Basin which locates at 40° latitude and 1.6km above sea level. Secondly, CH<sub>4</sub> concentration in Uintah Basin is much higher than typical background concentration due to oil and gas emission and strong inversions during winter time. Observed CH<sub>4</sub> at the Horsepool monitoring site during winter 2013 season reached as high as 20 ppm (Figure 2.2). A recent greenhouse gas measurement campaign led by researchers from University of Utah in Uintah Basin showed that CH<sub>4</sub> concentration in early summer 2015 was topping about 4 – 5 ppm (Figure 2.2) which is higher than typical background concentration. Even though no measurements have been made in winter time from this campaign, it is reasonable to assume that CH<sub>4</sub> concentrations would reach above 20 ppm in winter when the mixing height is shallow (< 100m). Lastly, products of reactions (R10) through (R13) include radicals and formaldehyde which have high O<sub>3</sub> reactivity. Our sensitivity study showed that a small increase in HCHO emission significantly increased O<sub>3</sub> formation (Tran et al. 2014).

Due to the unique conditions of winter ozone in the Uintah Basin, we believe that CH<sub>4</sub> chemistry becomes important for O<sub>3</sub> formation. Therefore we included reactions (R10) to (R13) in the SAPRC07 mechanism. Furthermore, we made CMAQ simulate CH<sub>4</sub>, i.e. CH<sub>4</sub> concentration is treated as a dynamical variable instead of keeping it at a constant concentration of 1.8 ppm as in the unmodified SAPRC07 mechanism.

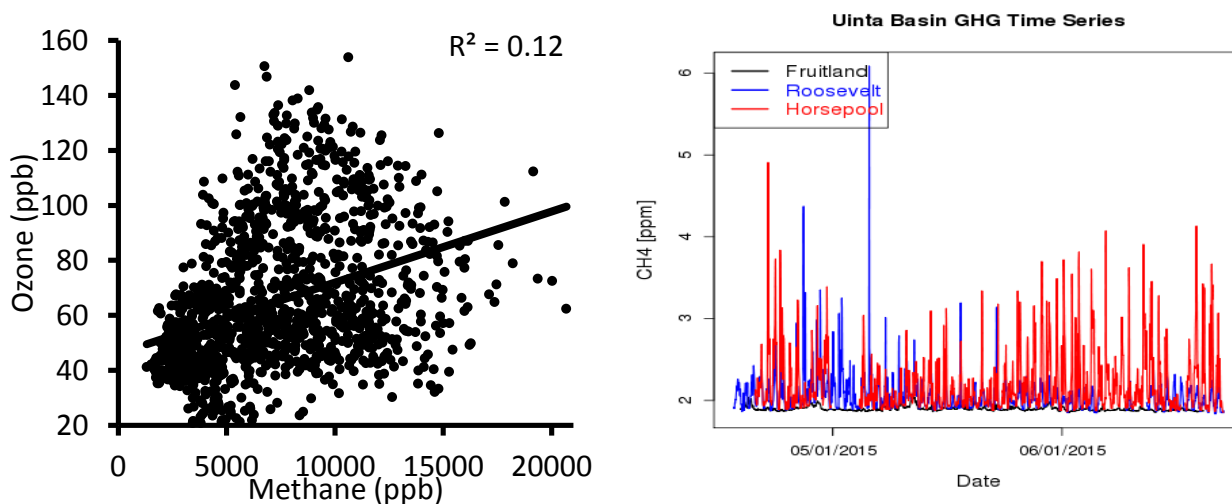


**Figure 2.2.** (Left) Relationship between observed O<sub>3</sub> and CH<sub>4</sub> concentration at Horsepool monitoring site in winter 2013 (Courtesy to Seth Lyman); (Right) Observed CH<sub>4</sub> concentrations at monitoring sites in the Uintah Basin during May and June 2015 (Courtesy to John Lin).

**Table 2.2.** Updates made to non-photolysis reactions in SAPRC07

ID <sup>a</sup>	Reaction description <sup>b</sup>	<i>k</i> (T)- Before update <sup>c</sup>	<i>k</i> (T) - after update <sup>c</sup>	References
<2>	O3P + O2 + M = O3	5.68e-34 <sup>-2.60</sup>	6.00e-34 <sup>-2.4</sup>	Sander et al. 2011
<5>	O3P + NO2 = NO	5.50e-12@-188	5.10e-12@-210	Sander et al. 2011
<7>	O3 + NO = NO2	3.00e-12@1500	2.07e-12@1400	IUPAC 2015
<8>	O3 + NO2 = NO3	1.40e-13@2470	1.20e-13@2450	Sander et al. 2011

ID <sup>a</sup>	Reaction description <sup>b</sup>	$k(T)$ - Before update <sup>c</sup>	$k(T)$ - after update <sup>c</sup>	References
<9>	NO + NO3 = 2*NO2	1.80e-11@-110	1.50e-11@-170	Sander et al. 2011
<21>	O1D + M = O3P	2.38e-11@-96	3.30e-11@-55	Sander et al. 2011
<22>	OH + NO = HONO	7.00e-31^-2.60 & 3.60e-11^-0.10 & 0.60 & 1.0	7.40e-31^-2.40 & 3.30e-11^-0.30 & 0.81 & 0.866	IUPAC 2015
<24>	OH + HONO = NO2	2.50e-12@-260	1.80e-11@390	Sander et al. 2011
<25>	OH + NO2 = HNO3	1.48e-30^-3.00 & 2.58e-11 & 0.60 & 1.0	3.2e-30^-4.50 & 3.00e-11 & 0.41 & 1.24	IUPAC, 2012
<26>	OH + NO3 = HO2 + NO2	2.00e-11	2.20e-11	Sander et al. 2011
<31>	HO2 + NO = OH + NO2	3.60e-12@-270	3.30e-12@-270	Sander et al. 2011
<32>	HO2 + NO2 = HNO4	2.00e-31^-3.40 & 2.90e-12^-1.10 & 0.60 & 1.0	1.40e-31^-3.10 & 4.00e-12 & 0.40 & 1.255	IUPAC 2015
<33>	HNO4 = HO2 + NO2	3.72e-05^-2.40@10650 & 5.42e+15^-2.30@11170 & 0.60 & 1.0	4.10e-05@10650 & 6.00e+15@11170 & 0.40 & 1.255	IUPAC 2015
<39>	NO3 + HO2 = 0.8*OH + 0.8*NO2 + 0.2*HNO3	4.00e-12	3.50e-12	Sander et al. 2011
<45>	OH + H2 = HO2	7.70e-12@2100	2.80e-12@1800	Sander et al., 2011
<BP72>	HOCCHO + OH = MECO3	1.0*K<BP08>	3.10e-12@-340	IUPAC 2015
<BP08>	CCHO + OH = MECO3	4.40e-12@-365	4.63e-12@-350	Sander et al. 2011
<BE03>	ETHENE + O3 = 0.16*HO2 + ...	9.14e-15@2580	1.20e-14@2630	Sander et al. 2011
<LT01> <sup>d</sup>	HO2 + NO = HNO3	N/A	6.40e-17@-1644	Butkovskaya et al., 2005
<LT02>	HO2 + NO + H2O = HNO3	N/A	8.96e-38@-3844	Butkovskaya et al., 2005
<LT03>	CH4 + O1D = OH + MEO2	N/A	1.05e-10	IUPAC 2015
<LT04>	CH4 + O1D = CH2OH + HO2	N/A	3.45e-11	IUPAC 2015
<LT05>	CH4 + O1D = HCHO	N/A	7.5e-12	IUPAC 2015
<LT06>	CH2OH + O2 = HCHO + HO2	N/A	5.33e-12@-170	Schocker et al. 2007

<sup>a</sup> Reaction ID is as defined in the SAPRC07 mechanism

<sup>b</sup> Chemical species are notated as in SAPRC07 mechanism

<sup>c</sup> For CMAQ model application, the reaction rate  $k(T)$  is notated as  $k(T)=A^B@C$ , which represents the expression  $k(T) = A \cdot (T/300)^B \cdot e^{-C/T}$ , where  $C = E_a/R$ . Units of  $k$  and  $A$  are  $\text{cm}^3 \cdot \text{molec}^{-1} \cdot \text{s}^{-1}$ ,  $E_a$  are  $\text{kcal} \cdot \text{mol}^{-1}$ ,  $T$  is Kelvin, and  $R = 0.0019872 \text{ kcal} \cdot \text{mol}^{-1} \cdot \text{K}^{-1}$ . Omitted parameter in an expression means such parameter equals zero. In reactions where more than one notation of  $A^B@C$  or additional parameters are given,  $k(T)$  is described in different temperature and pressure dependent expressions. See Carter (2010) for more details.

<sup>d</sup> Reactions <LT01> through <LT06> are newly added to SAPRC07 in this study.

**Table 2.3.** Updates from SAPRC11 that are implemented to SAPRC07T <sup>a</sup>

ID	SAPRC07		SAPRC11	
	Reaction description	$k(T)$	Reaction description	$k(T)$
<BR22>	MECO3 + HO2 = products	5.20e-13@-980	MECO3 + HO2 = products	5.20e-13@-981
<BR32>	RCO3 + HO2 = products	Same as <BR22>	RCO3 + HO2 = products	Same as <BR22>
<BR43>	BZCO3 + HO2 = products	Same as <BR22>	BZCO3 + HO2 = products	Same as <BR22>
<BR55>	MACO3 + HO2 = products	Same as <BR22>	MACO3 + HO2 = products	Same as <BR22>
<BP32> <sup>b</sup>	GLY + OH = products	1.10e-11	GLY + OH = products	3.10e-12@-342
<BP33>	GLY + NO3 = products	2.80e-12@2376	GLY + NO3 = products	2.80e-12@2376
<BP38> <sup>b</sup>	CRES + OH = products	1.70e-12@-950	CRES + OH = products	1.60e-12@-971
<BP39> <sup>b</sup>	CRES + NO3 = products	1.40e-11	CRES + NO3 = products	1.40e-11
<BP47>	AFG1 + O3 = products	9.66e-18	Removed	
<BP50>	AFG2 + O3 = products	9.66e-18	Removed	
<BE10>	ACETYLENE + OH = products	5.50e-30 <sup>-2.00</sup> & 8.30e-13 & 0.60 & 1.0	ACETYLENE + OH = products	5.50e-30 & 8.30e-13 <sup>-2.0</sup> & 0.60 & 1.0
<SA01> <sup>c</sup>	N/A		HCOCO3 + NO = products	Same as <BR31>
<SA02>	N/A		HCOCO3 + NO2 = products	Same as <BR28>
<SA03>	N/A		HCOCO3 + HO2 =	Same as <BR22>
<SA04>	N/A		CATL + OH = products	2.00e-10
<SA05>	N/A		CATL + NO3 = products	1.70e-10

<sup>a</sup> Not all updates made in SAPRC11 mechanism have been implemented in SAPRC07 in this study

<sup>b</sup> New species have been introduced in SAPRC11 and they are introduced in the updated SAPRC07 in this study.

<sup>c</sup> Reactions <SA01> through <SA05> are newly introduced in SAPRC11 and are implemented into SAPRC07 in this study.

## 2.2. Model setups

### 2.2.1. Meteorological model

We employed the Weather Research and Forecasting (WRF; Skamarock et al. 2008) version 3.5 as the meteorological model to generate the meteorological inputs required for the CMAQ photochemistry model. WRF model simulations were performed on one-way nested domains which consist of an outer domain at 12 km horizontal resolution covering the entire western USA, an inner domain at 4-km horizontal resolution covering Utah and adjacent states, and a high-resolution domain at 1.3-km horizontal and centered at the Uintah Basin (Figure 2.3). Vertical resolution was constructed with 40 vertical layers reaching 15km (100 mbar) at the top layer (Table 2.4). Model outputs for the 1.3 km-resolution domain were used as inputs for CMAQ runs.

We adapted well-tested WRF model configurations for the Uintah Basin winter weather conditions (Neemann et al. 2015). As such, the following physical schemes were selected: the Thompson cloud microphysics scheme (Thompson et al. 2008) with modifications; the Kain-Fritsch cumulus ensemble scheme (Kain 2004) for the 12 km domain only; the treatment of long-wave and short-wave radiation based on Iacono et al. (2008); the Mellor Yamada Janjić scheme (MYJ; Janjić 1994) for the atmospheric boundary layer (ABL); and the Noah scheme (Chen and Dudhia 2001) for the land surface model. Initial and boundary conditions for WRF simulations at 12 km domain were generated from the North American Mesoscale Model analysis data (<http://www.emc.ncep.noaa.gov/index.php?branch=NAM>).

## **Modifications made to WRF physical packages**

### ***Snow Initial Conditions***

Snow albedo is a key factor driving photochemical reactions as well as physical processes in the ABL. Therefore, WRF performance in simulating snow cover is highly important. Initializing snow field data (i.e., snow depth and water equivalent) with NAM 12-km analysis data resulted in a too coarse snowfield. To better resolve snow field data, we adapted the Snow Data Assimilation System (SNOWDAS; NOHRSC 2004) 30 arc seconds resolution data for initializing WRF simulations. Further treatment was applied to grid-cells in the Uintah Basin where snow fields data were replaced with observational data following Neemann et al. (2015)'s modifications. Our sensitivity study showed that this snow initialization resulted in significant improvement in snow depth and snow albedo performance in comparison with snow initialization with NAM 12-km analysis data.

### ***Cloud Physics***

We adapted modifications introduced by Neemann et al. (2015) to the Thompson microphysics scheme. These modifications switched off cloud-ice sedimentation and the auto-conversion of cloud ice to snow and by that kept low ice-cloud suspended and persistent in the air. This modification resulted in better agreement with observation in an episode when there was clear evidence of fog rather than clouds (Crossman E., 2013, per. comm.) and may not be applicable for other episodes.

### ***Vegetation:***

Our independent project with the researcher in the University of Utah suggested that using the US Geological Survey 33 categories (USGS-33) land-use scheme provided the best results of all tested land-use schemes in term of snow cover performances. Furthermore, the vegetation tables used in the WRF model for the Uintah Basin needed to be modified in order to decrease the effective depth of the grass by several inches to better represent the sparse, short grasses observed in the Basin. Thus, we modified the vegetation tables of the USGS-33 land-use scheme accordingly

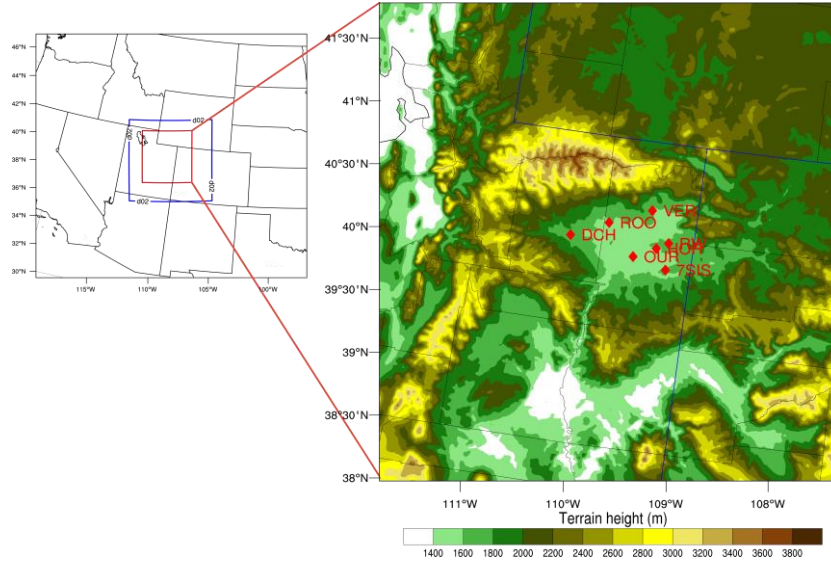


**Figure 2.3.** WRF and CMAQ model domain configuration. The grid-cell counts for the 12 km, 4 km and 1.3 km domain are 180 x 168, 165 x 168, and 297 x 321, respectively. CMAQ simulations were performed at the WRF 1.3 km domain less six grid-cells at each of its lateral boundaries (i.e., 285 x 309 grid-cells). Locations of monitoring sites including Duchesne (DCH), Roosevelt (ROO), Vernal (VER), Ouray (OUR), Horsepool (HOR), Red Wash (RW), and Seven Sister (7SIS) are indicated in the figure.

**Table 2.4.** Vertical layer structure for Uintah Basin air quality modeling simulations.

WRF MODEL LAYER	CMAQ MODEL LAYER	$\eta$ LEVEL	HEIGHT ABOVE SURFACE* (m)
40 (Top)	21	0.050	15091
39		0.100	12907
38		0.150	11238
37	20	0.200	9905
36		0.250	8804
35		0.300	7852
34	19	0.350	7003
33		0.400	6229
32		0.450	5518
31	18	0.500	4857
30		0.550	4241
29		0.600	3663
28	17	0.650	3119
27		0.700	2605
26		0.740	2213
25	16	0.770	1929
24		0.800	1654
23		0.820	1475
22	15	0.840	1299
21		0.860	1126
20		0.880	956
19	14	0.900	789
18		0.910	707
17		0.920	626
16	13	0.930	545
15		0.940	465

WRF MODEL LAYER	CMAQ MODEL LAYER	$\eta$ LEVEL	HEIGHT ABOVE SURFACE* (m)
14	12	0.950	385
13		0.955	346
12	11	0.960	307
11		0.965	268
10	10	0.970	229
9	9	0.975	190
8	8	0.980	152
7	7	0.983	133
6	6	0.985	114
5	5	0.988	94
4	4	0.990	75
3	3	0.993	53
2	2	0.995	38
1	1	0.998	18
0(ground/surface)	0	1.000	0

\* Altitude above sea level is estimated according to standard atmosphere assumptions: sea-level pressure of 1,000 mbar, model top at 100 mbar, surface temperature of 275 degrees Kelvin ( $^{\circ}$ K), and lapse rate of  $50^{\circ}$ K/ natural log-pressure ( $\ln[p]$ ).

### 2.2.3. CMAQ model

We employed the CMAQ model (Byun and Schere 2006) version 5.0.2 as the photochemical model to evaluate the effect of the modified SAPRC07 mechanism on winter  $O_3$  simulation in the Uintah Basin. CMAQ simulations were performed on the WRF 1.3 km domain (Figure 2.3) and with 21 vertical layers (Table 2.4). In addition to modifications made to the SAPRC07 chemical mechanism, we performed improvement to the CMAQ physical packages as discussed in the following sections.

#### **Snow albedo**

Snow albedo calculated by the WRF model is not passed along to CMAQ. Rather, CMAQ calculates snow albedo as a function of land-use, season, time of day and wavelength. Currently, the CMAQ photolysis module does not support the USGS-33 land-use scheme and CMAQ's default albedo values resulted in an unrealistic spatial distribution of surface albedo in the model domain (Figure 2.4). We modified the CMAQ photolysis module to support USGS-33. This improvement resulted in surface albedos that represent well the land use characteristics and reproduce the spatial distribution estimated by WRF (Figure 2.4). This increase in surface albedo led to an increase in the  $O_3$  formation rate.

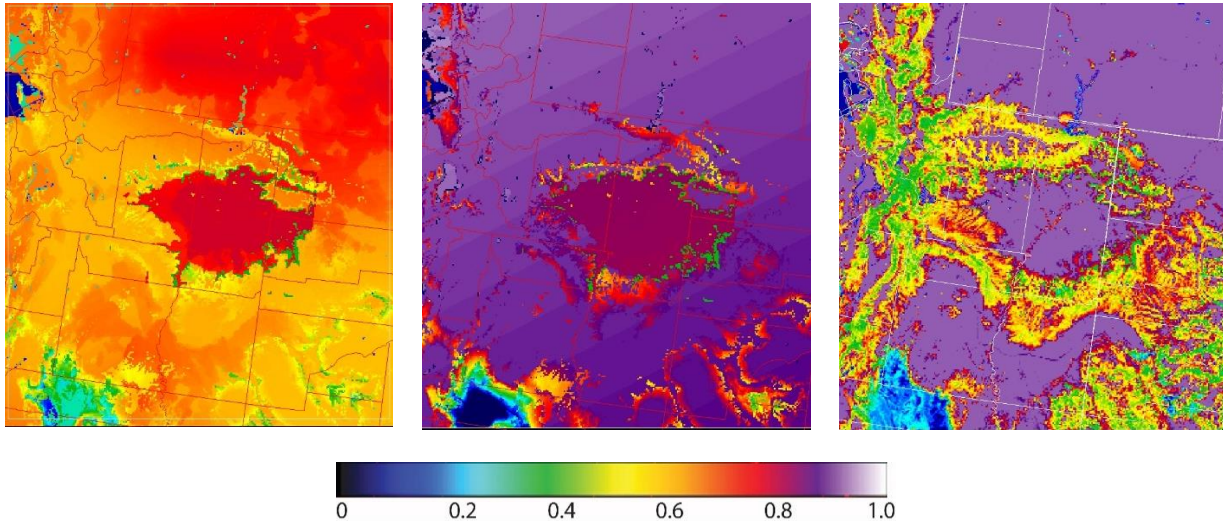


**Figure 2.4.** Surface albedos as estimated by (from left to right) WRF, unmodified CMAQ, and modified CMAQ.

***Improvement in dry deposition of chemical species onto the snow surface.***

The CMAQ dry deposition module estimated dry deposition velocity at about +0.09 cm/s. Meanwhile, measurements of dry deposition velocity of O<sub>3</sub> onto snow-covered surfaces in the Uintah Basin to be 0.003 cm/s at the median with a 2-σ window ranging from -0.071 to +0.079 cm/s during daytime (Helmig et al. 2014). Overestimation of dry deposition velocity leads to underestimation of chemical concentrations in the atmosphere.

Recent study by Helmig et al. (2014) showed that over snow surface O<sub>3</sub> has very low dry deposition velocity which is also much lower than the CMAQ-calculated dry deposition velocity. Using the surface-specific resistance values reported by Helmig et al. (2007) and Zhang et al. (2003), we modified the CMAQ dry deposition module at the source-code level. The modified module estimated O<sub>3</sub> dry deposition velocities to be about half that of the unmodified module (Figure 2.5). The net effect of this modification is to increase O<sub>3</sub> concentration in the atmosphere due to less O<sub>3</sub> deposition to the surface.

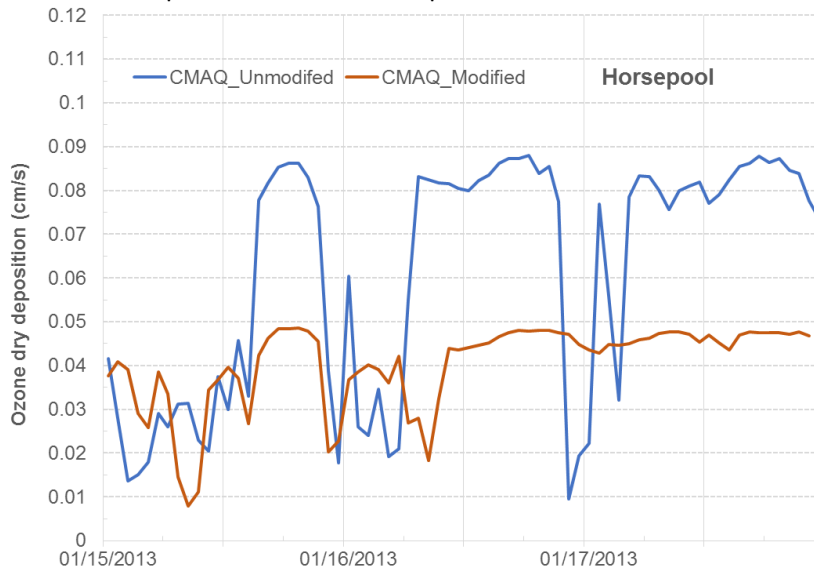


**Figure 2.5.** O<sub>3</sub> dry deposition velocity as simulated at the Horsepool monitoring site by the unmodified and modified CMAQ models.

***Model source code modifications to accommodate the updated SAPRC07 mechanism.***

We modified the CMAQ photolysis module and chemical solver to facilitate the updates to SAPRC07 as discussed in earlier sections. The modified source codes are attached and explained in separate documents.

**2.2.4. Emission model**

We adopted Uintah Basin emissions inventories that were developed under the Air Resource Management Strategy (ARMS-EI) of the Utah office of the Bureau of Land Management (AECOM 2014). Where appropriate, we updated the ARMS-EI (base year 2010) with the NEI 2011. Other updates to ARMS-EI include extrapolation of oil and gas emissions and production growth rate data from base year 2010 to model year 2013 using scale factors derived from well counts.

We used the Sparse Matrix Operator Kernel Emissions (SMOKE) model (Houyoux and Vukovich 1999) to process the ARMS-EI data for the CMAQ model (Figure 2.6). We developed spatial surrogates to allocate all emissions to the model domain at 1.3-km horizontal resolution (Figure 4.1) using ArcGIS software with the most recent data from the Census Bureau, the Federal Emergency Management Agency (FEMA), the National Land Cover Dataset, the Utah Division of Oil, Gas, and Mining (UDOGM), and other sources. Default SMOKE temporal surrogates and temporal surrogates developed by AECOM for the ARMS-EI (AECOM, 2013) accounting for oil and gas activities were adopted for the Uintah Basin model domain.

The SMOKE defaults provide no VOC speciation profiles for the SAPRC07 chemical mechanism. Several VOC speciation profiles are being shared among SMOKE's users but they are only applicable for the SAPRC99 mechanism, an earlier version of SAPRC07. To develop VOC speciation profiles, we utilized the U.S. EPA Speciate 4.4 database processed with the Improved Chemical Speciation Database (Carter 2015). The developed VOC speciation profiles for SAPRC07 share the same profile identification numbers and thus profile assignments with the CB05 chemical mechanism.

We tested different sets of VOC speciation profiles and evaluated their effects on simulating winter O<sub>3</sub> concentration in the Uintah basin (Tran et al. 2014). The sensitivity study showed that VOC profiles that account for high formaldehyde emission from oil and gas activities (e.g., flaring) resulted in high estimated O<sub>3</sub> concentrations in comparison with other VOC profiles. This finding agrees well with findings from other studies (e.g., Avey et al. 2015). However, for the purpose of this study, we applied the default VOC profile assignments as recommend by the Western Regional Air Partnership phase III (WRAP-III) study for oil and gas emissions. These VOC speciation assignments are known to result in underestimation of O<sub>3</sub> concentrations (Tran et al. 2014). For oil and gas emission categories without WRAP-III recommendations, where appropriate we adopted several VOC speciation profiles developed for oil and gas activities in the states of Texas and Wyoming.

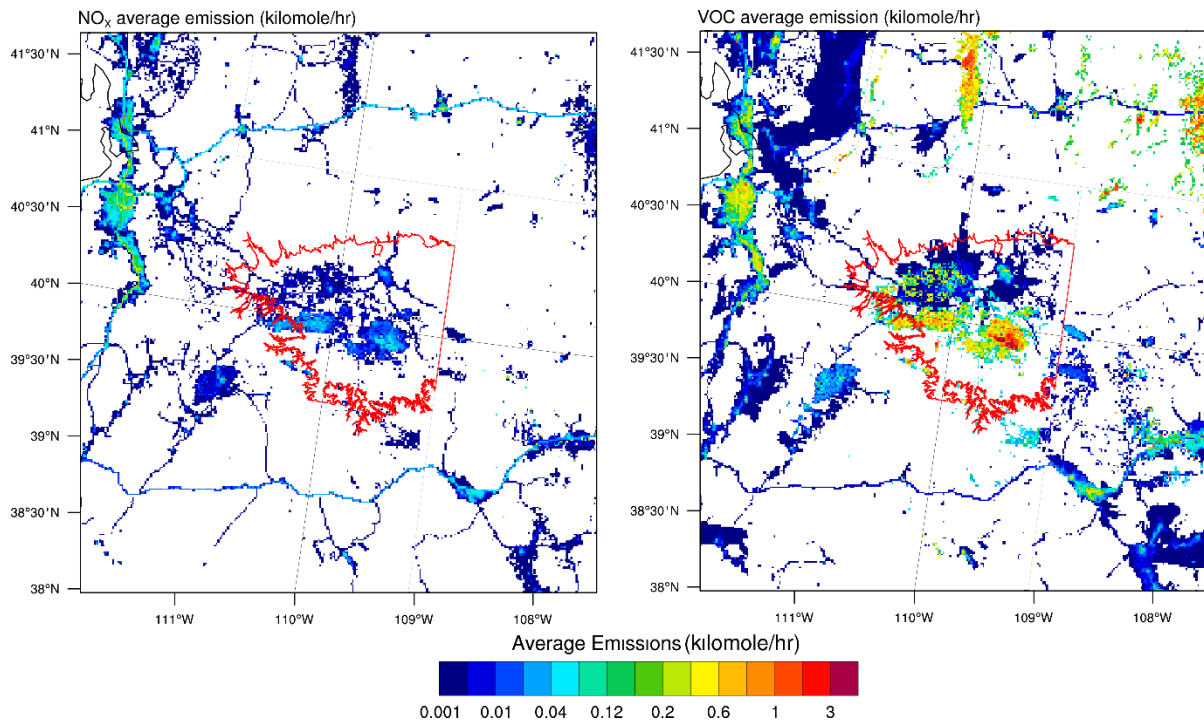


**Figure 2.6.** Average NO<sub>x</sub> and VOC emissions as processed by the SMOKE emissions model based on the updated ARMS-EI data. Red polyline depicts the Uintah Basin.

### 3. MODELING EPISODES AND SENSITIVITY SIMULATIONS

We performed WRF-CMAQ simulations for an episode of 29 January – February 8, 2013 when observed O<sub>3</sub> concentrations from several monitoring stations exceeded the National Ambient Air Quality Standard (NAAQS) of 75 ppb (Figure 3.1). This episode starts with the passage of a new high-pressure system over Utah in 29 January following the storm events of 27 - 28 January, 2013. Stagnant and light wind conditions gradually built up that led to O<sub>3</sub> concentrations exceeding the NAAQS starting from 31 January to 8 February when O<sub>3</sub> concentration decreased due to mixing conditions caused by the passage of a low-pressure system. These high- and low-pressure systems were reproduced by WRF over the simulation domain.

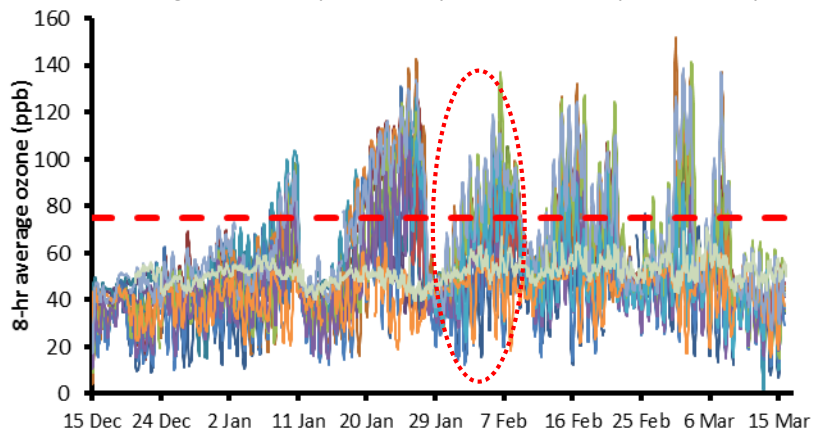


**Figure 3.1.** Time series of ozone concentration (ppb) at eight monitoring sites within the Uintah Basin, January through mid-March 2013 (Lyman et al., 2013) with the simulated episode enclosed in red-dot circle.

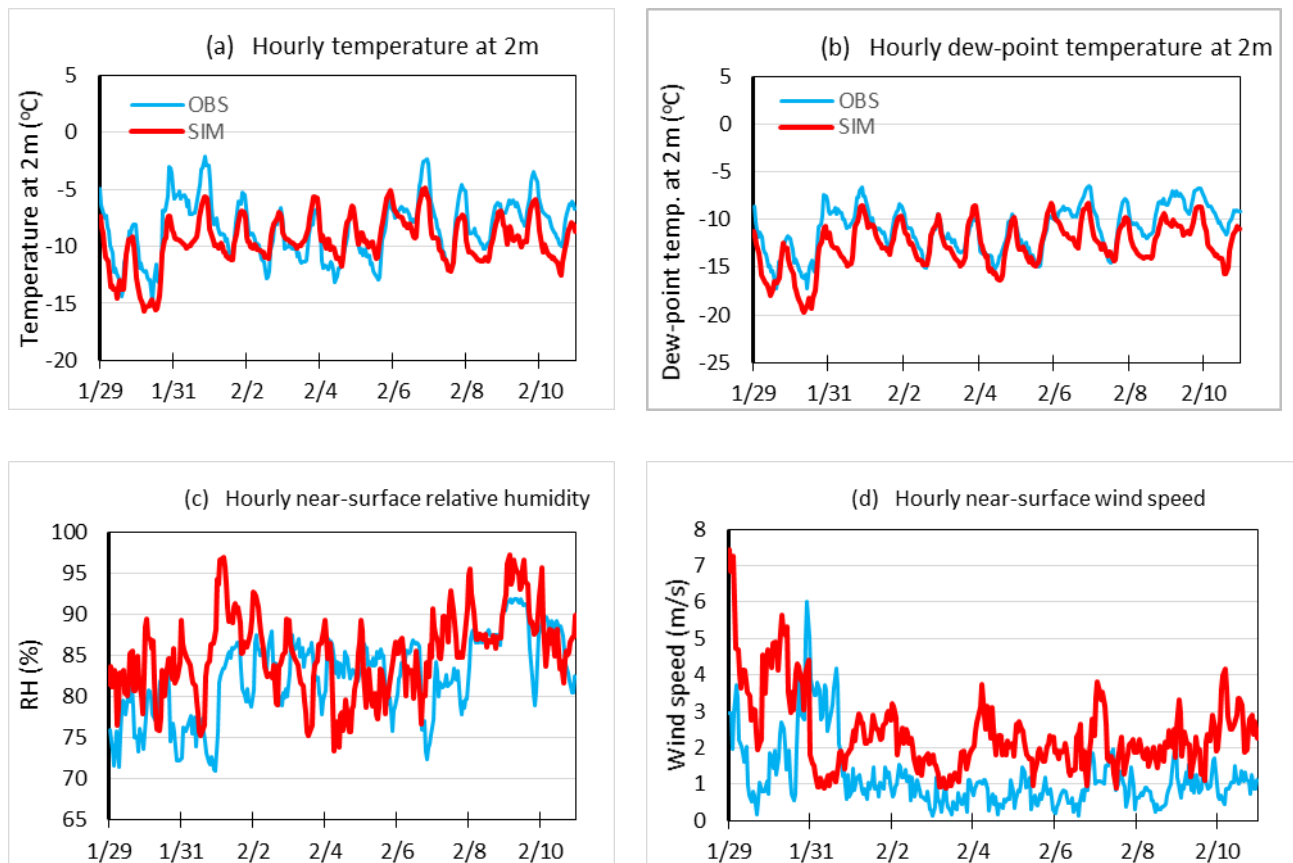
We performed four sets of CMAQ sensitivity simulations to evaluate the effect of the updated SAPRC07 mechanism on O<sub>3</sub> concentration: the REF simulation with non-updated SAPRC07 mechanism; the NITRIC

and METHAN simulations with SAPRC07 mechanism updated with only HNO<sub>3</sub> branching effect and CH<sub>4</sub> chemistry, respectively; finally, the ALLUPD simulation with SAPRC07 mechanism with all updates as discussed in earlier sections.

## 4. MODEL PERFORMANCE

### 4.1. WRF Model

Comparison of WRF simulated vs. observed air temperature ( $T$ ), dew-point temperature ( $T_d$ ), relative humidity (RH), wind speed ( $v$ ) and wind direction ( $v_{dir}$ ) are shown in the Figure 4.1. Mean biases for  $T$ ,  $T_d$ , RH,  $v$ , and  $v_{dir}$  throughout the episodes are  $-1.10$  °C,  $-1.70$  °C, 2.73 %, 1.20 m/s and 39°; respectively. More details on the skill-score performance are presented in Table 4.1. Discrepancies in simulating wind fields are common in mesoscale models, especially with complex terrain as in the Uintah Basin. Overall, our WRF simulations have good performance in simulating a number of meteorological properties as well as well capturing the timing of the formation and breakup of the inversions.



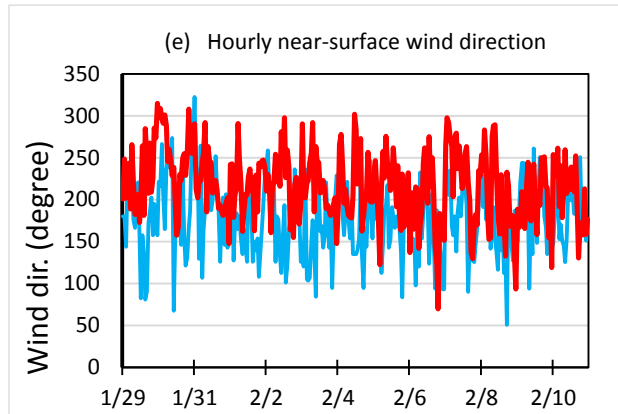


**Figure 4.1.** Comparison of simulated (red) and observed (blue) meteorological quantities throughout the simulated episode. The presenting values are averaged over seven meteorological stations in the Uintah Basin.

**Table 4.1.** WRF performance statistics.

Parameter	Statistic	General Benchmark*	Complex Terrain Benchmark**	Average Values***
<b>v (m/s)</b>	RMSE <sup>1</sup>	≤2	≤ 2.5	1.70
	Bias <sup>2</sup>	≤±0.5	NA	1.20
	IOA <sup>3</sup>	≥0.6	NA	0.86
<b>v<sub>dir</sub> (deg)</b>	Bias	≤±10	NA	39.74
	Gross Error <sup>4</sup>	≤30	≤55	39.99
<b>T (C)</b>	Bias	≤±0.5	≤±2	-1.10
	Gross Error	≤2	≤3.5	1.75
	IOA	≥0.8	NA	0.93

\* Tesche et al. 2002

\*\* Kemball-Cook et al. 2005; N/A = not applicable (i.e., no complex-terrain benchmark is available).

\*\*\* Red indicates data that pass both general and complex terrain benchmarks. Blue indicates data that pass only the complex terrain benchmark, and black indicates data that fail both benchmarks.

<sup>1</sup>  $RMSE = \left[ \frac{1}{MN} \sum_{j=1}^N \sum_{i=1}^M (P_{ij} - O_{ij})^2 \right]^{1/2}$  where  $P_{ij}$  and  $O_{ij}$  are the simulated and observed quantities over  $M$  number of time points and  $N$  number of monitoring station, respectively.

<sup>2</sup>  $Bias = \frac{1}{MN} \sum_{j=1}^N \sum_{i=1}^M P_{ij} - O_{ij}$

<sup>3</sup>  $Index\ of\ Agreement\ (IOA) = 1 - \left[ \frac{MN \times RMSE^2}{\sum_{j=1}^N \sum_{i=1}^M (|P_{ij} - M_o| + |O_{ij} - M_o|)} \right]$  where  $M_o$  is the mean of observation quantities

<sup>4</sup>  $Gross\ Error = \frac{1}{MN} \sum_{j=1}^N \sum_{i=1}^M |P_{ij} - O_{ij}|$

## 4.2. CMAQ Model Performance

CMAQ captures the temporal evolution of  $O_3$  concentrations at all monitoring stations except at Horsepool, and highly underestimated  $O_3$  concentrations at all stations throughout the simulation episode (Figure 4.2, Table 4.2). The largest discrepancies between observed and simulated  $O_3$  occurred at monitoring stations that are located in areas with high oil and gas activities (e.g., Ouray, Horsepool). Errors in simulating meteorological quantities (especially wind fields) and discrepancies in the emission inventory are the causes for CMAQ's weak  $O_3$  performance. We attribute the latter cause as the main factor. Our

independent sensitivity analysis showed that using the same WRF-simulated meteorological inputs, CMAQ had better O<sub>3</sub> performance with EI that accounts for high formaldehyde emission than with the EI with low formaldehyde emission (Tran et al. 2014).

At Vernal, CMAQ underestimated daytime O<sub>3</sub> concentration. Additionally, CMAQ underestimated nighttime O<sub>3</sub> titration at this site (Figure 4.1.). Our sensitivity analysis showed that a CMAQ simulation with different EI did not result in a significant difference in O<sub>3</sub> performance at this site (Tran and Tran 2015). Errors in simulating meteorological quantities are the minor cause for the weak O<sub>3</sub> performance at this station.

CMAQ's underestimation of O<sub>3</sub> concentration and its sensitivity to formaldehyde emission agrees well with findings from other studies (e.g., Avey et al. 2015; Emery and Yarwood 2015).

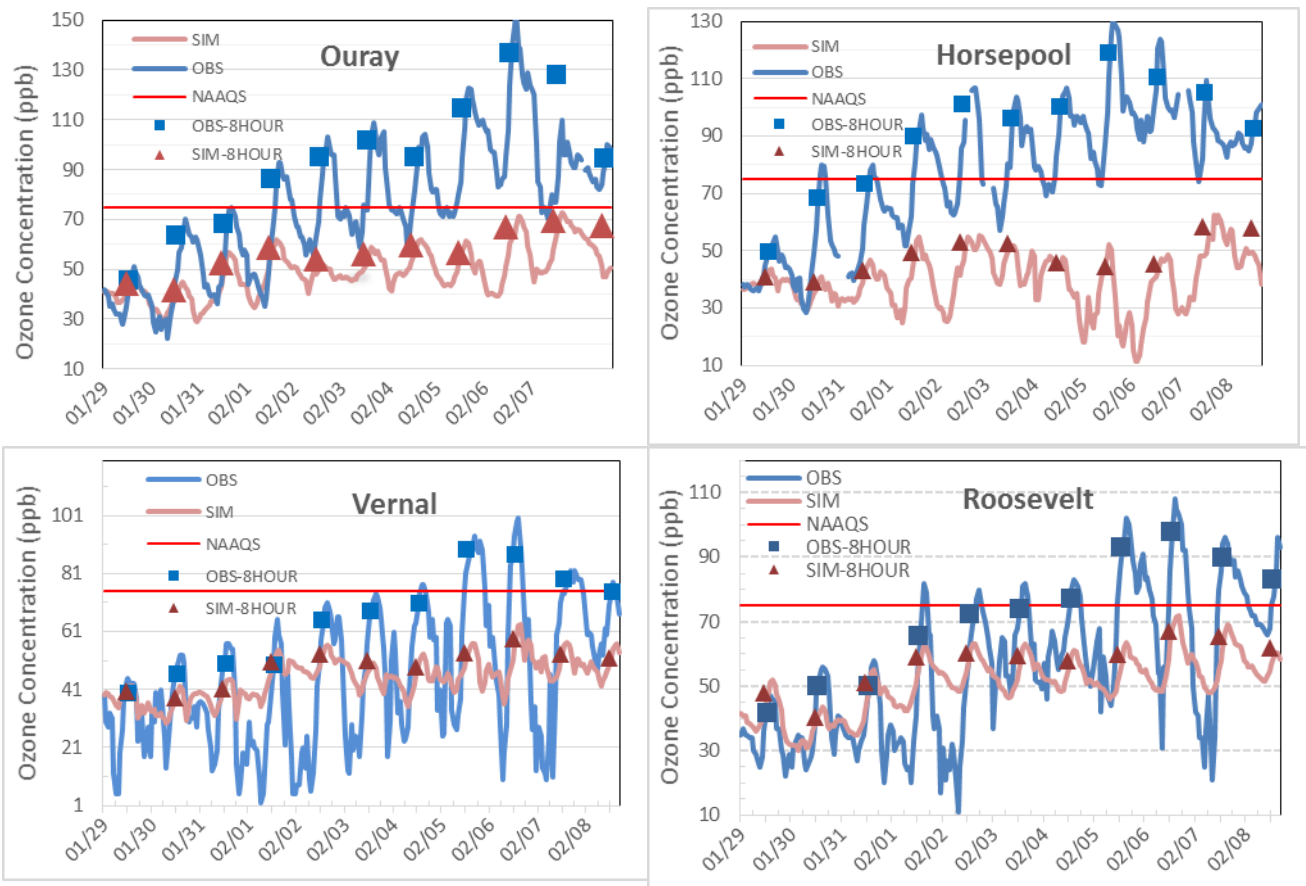


**Figure 4.2.** Comparison of simulated (SIM) vs. observed (OBS) O<sub>3</sub> concentrations at four monitoring stations in the Uintah Basin.

**Table 4.2.** CMAQ performance skill-scores

Station	Quantity	MNB(%) <sup>1</sup>	MNGE(%) <sup>2</sup>	Correlation
Horsepool	Hourly concentrations	-43.1	43.1	0.157
	Daily 8-hour maxima	-45	45	0.489
Ouray	Hourly concentrations	-27.7	30.9	0.747
	Daily 8-hour maxima	-35.9	35.9	0.827
Red Wash	Hourly concentrations	-35.2	37.3	0.036
	Daily 8-hour maxima	-17.9	36.8	0.874
Vernal	Hourly concentrations	56.3	79.9	0.615
	Daily 8-hour maxima	-22.2	22.6	0.851
Roosevelt	Hourly concentrations	4.4	27.9	0.794
	Daily 8-hour maxima	-17.9	20.8	0.874

$$^1 \text{ Mean Normalized Bias (MNB)} = \frac{1}{M} \sum_{i=1}^M \left( \frac{P_i - O_i}{O_i} \times 100\% \right)$$

$$^2 \text{ Mean Normalized Gross Error (MNGE)} = \frac{1}{M} \sum_{i=1}^M \left( \left| \frac{P_i - O_i}{O_i} \right| \times 100\% \right)$$

## 5. RESULTS AND DISCUSSION

### 5.1. HNO<sub>3</sub> branching effect

As expected, including the HNO<sub>3</sub> branching effect into the SAPRC07 mechanism decreased O<sub>3</sub> production. However, the impact is marginal. At the surface layer, the greatest O<sub>3</sub> reduction was 0.96 ppb among all monitoring stations and occurred at Ouray. Total O<sub>3</sub> column concentrations, determined as the total O<sub>3</sub> concentration over a modeled grid-column (layer 0 – 21, Table 2.4), is as large as 4.7 ppb lower in NITRIC than in REF (Figure 5.1). O<sub>3</sub> reduction is greatest in areas with high oil and gas activities horizontally and 0 - 200 m above ground level (AGL). Above 200 m AGL, the effect of the HNO<sub>3</sub> branching ratio on O<sub>3</sub> reduction quickly decreases and has no impact above 1,300 m AGL.

During a high O<sub>3</sub> period, CMAQ underestimated HNO<sub>3</sub> concentration at Horsepool, which is the only station that measured HNO<sub>3</sub> during the simulation period (Figure 5.2). In comparison to REF, HNO<sub>3</sub> concentrations in NITRIC marginally increased (< 0.04 ppb). CMAQ also estimated an unnoticeable increase in nitrate aerosol concentrations (< 3%) in NITRIC over REF.

No clear relationship between temperature and HNO<sub>3</sub> formation was found. Rather, HNO<sub>3</sub> formation increases as NO<sub>x</sub> concentration increases under the existent inversion layer from January 29 to February 07, 2013. Longer simulation episodes should be performed to evaluate the temperature-HNO<sub>3</sub> negative relationship.

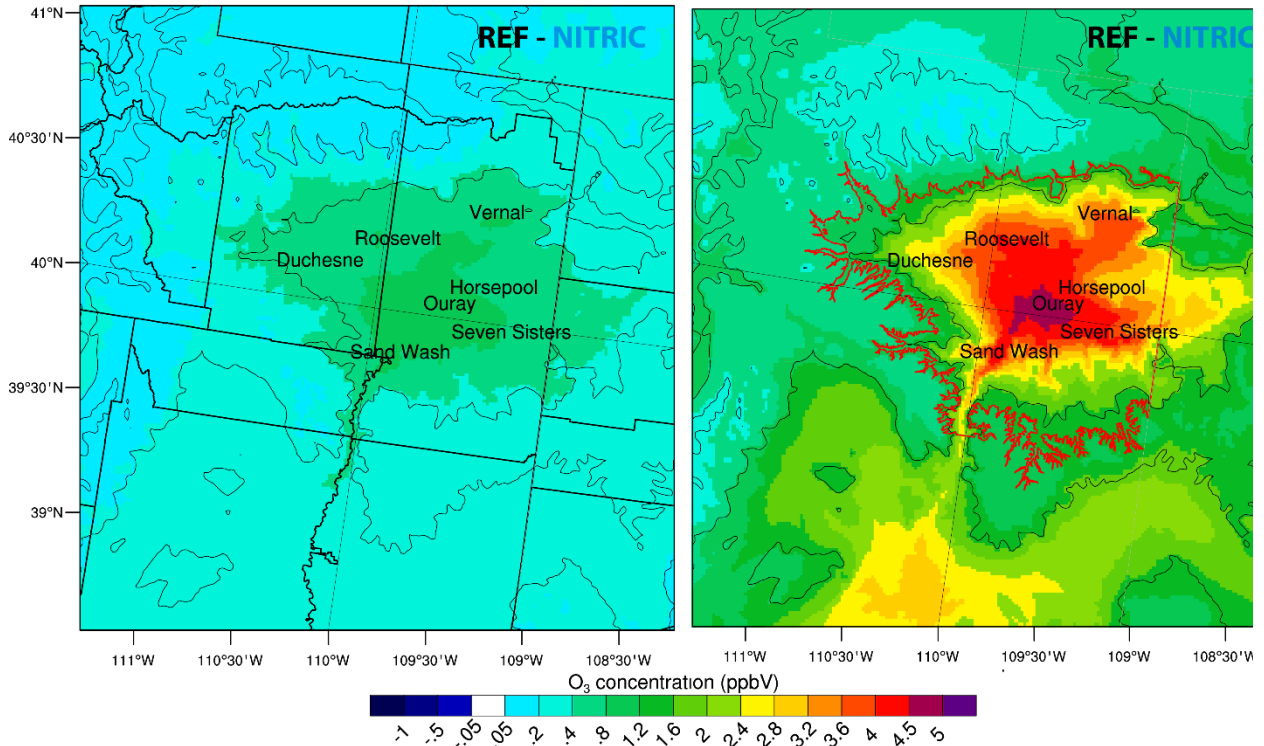


**Figure 5.1.** Highest O<sub>3</sub>-differences in REF and NITRIC (expressed as REF – NITRIC) over simulation period (left) at surface layer and (right) over total O<sub>3</sub> column–concentrations.

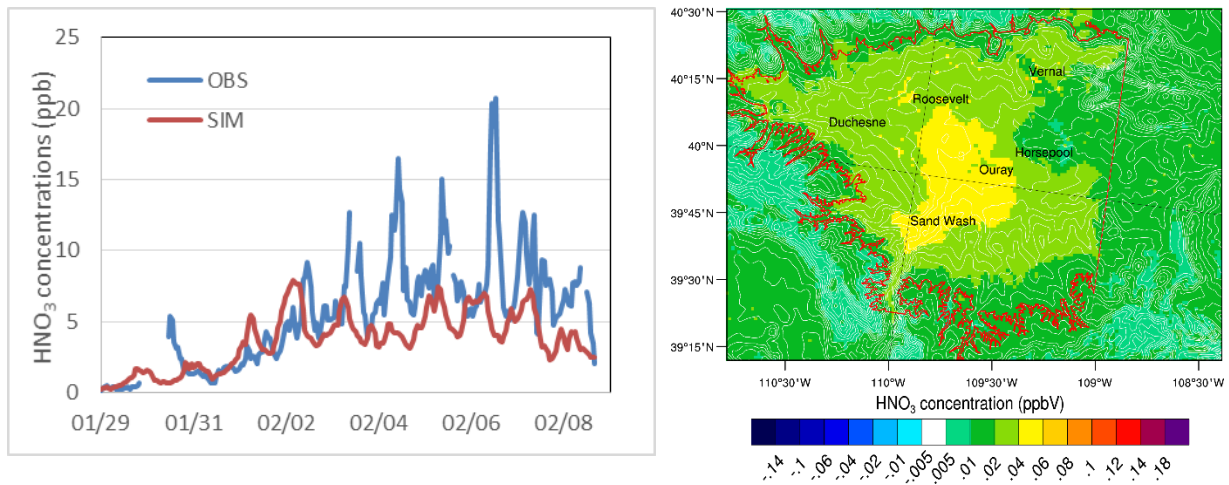


**Figure 5.2.** (left) Comparison of simulated vs. observed HNO<sub>3</sub> at Horsepool monitoring station; (right) HNO<sub>3</sub> highest-differences (NITRIC – REF) throughout simulation period.

## 5.2. CH<sub>4</sub> chemistry

Including CH<sub>4</sub> chemistry into the SAPRC07 mechanism in METHN increases O<sub>3</sub> formation over REF simulations (Figure 5.3). Among all monitoring sites in the Basin, the impact of CH<sub>4</sub> chemistry on O<sub>3</sub> formation is greatest at Ouray where O<sub>3</sub> concentration increases as much as 1.1 ppb. However, CH<sub>4</sub> chemistry has its greatest impact on O<sub>3</sub> formation over the coalbed methane gas field in Carbon and Emery counties where O<sub>3</sub> increases as much as 1.6 ppb at several locations (Figure 5.3). Note that in coalbed methane gas field, CH<sub>4</sub> accounts for larger partition of total VOC emissions than in the traditional oil and gas field of the Uintah Basin.

Total O<sub>3</sub> column-concentration increases up to 5.3 ppb as observed in the Uintah Basin and in coalbed methane gas field (Figure 5.3). The greatest impact of CH<sub>4</sub> chemistry on O<sub>3</sub> formation occurs within 0 – 100 m AGL. Above 550 m AGL, the impact quickly decreases and reaches zero-impact above 4,000 m AGL.

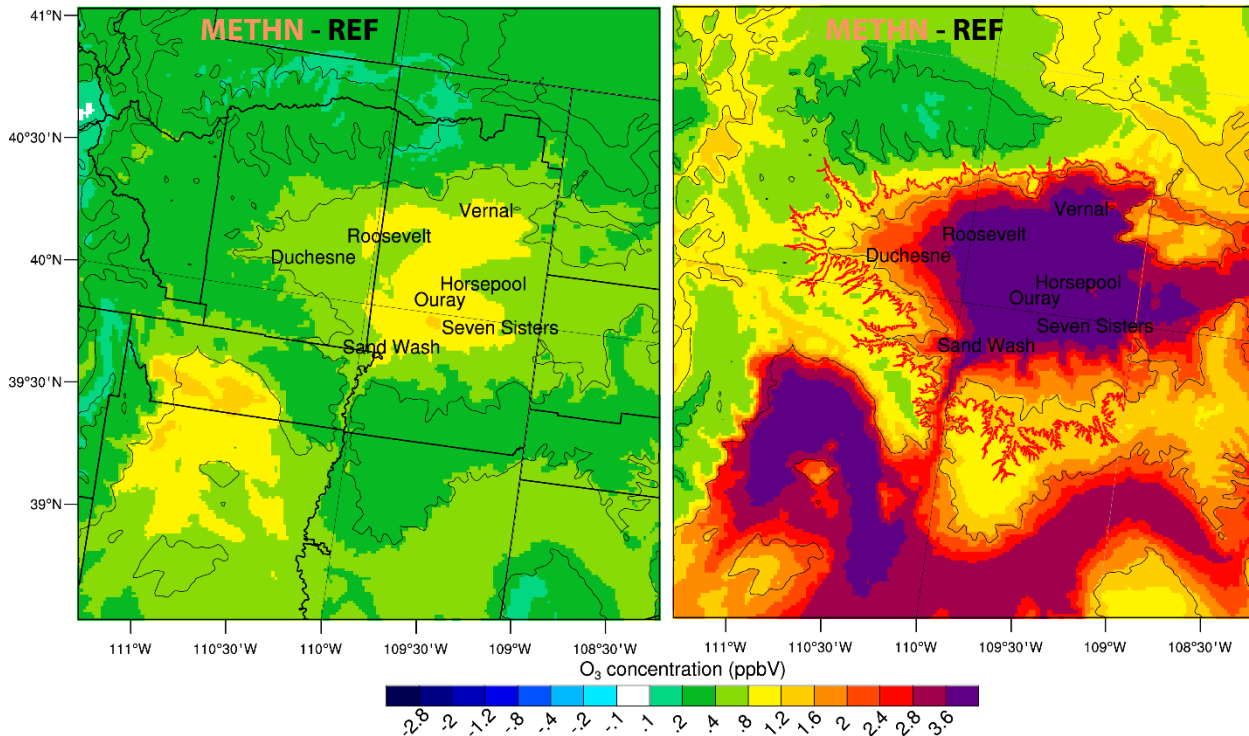


**Figure 5.3.** Analogous to Figure 5.1 but for METHN – REF O<sub>3</sub>-differences.

HO<sub>x</sub> and HCHO concentrations are higher in METHN than in REF both in daytime and nighttime. Although HO<sub>x</sub> (HO + HO<sub>2</sub>) radicals and HCHO concentrations increase in METHN over REF by very small amounts (< 0.3 ppt and < 50 ppt, respectively), the increases in METHN equal to 8% of HO<sub>x</sub> and 5% of HCHO concentrations on average in REF during daytime when photolysis reactions occur. Note that the simulated HO<sub>x</sub> and HCHO concentrations in the atmosphere are typically very low (~ 2 ppt and ~ 0.6 ppb on average, respectively) due to their high photochemical reactivity.

At Horsepool, the estimated CH<sub>4</sub> concentration is 2.4 ppm on average and 3.0 ppm at the maximum which is higher than typical background CH<sub>4</sub> concentrations (1.85 ppm). However, the CMAQ-estimated CH<sub>4</sub> concentration is significantly lower than observed (Figure 5.4). This finding is expected given our knowledge that not all emission sources are covered in the EI (e.g., fugitive emissions, soil seepage). Additionally, in model application CH<sub>4</sub> emission is calculated from the total VOC emissions using appropriate VOC speciation profiles. Due to the poor representativeness of the VOC speciation profiles, this is an additional layer of uncertainty in the CH<sub>4</sub> emission data used in photochemical models.

Due to the potential importance of CH<sub>4</sub> chemistry on O<sub>3</sub> formation in the Uintah Basin, we performed CMAQ simulations with CH<sub>4</sub> emissions arbitrarily increased by 10 times (METHNx10) to evaluate its impact on O<sub>3</sub>. The estimated CH<sub>4</sub> concentration in METHNx10 at Horsepool is 6.1 ppm on average and 12.0 ppm at the highest which is still lower than observation (Figure 5.4). However, O<sub>3</sub> concentrations in METHNx10 significantly increase over REF. In comparison with REF, surface O<sub>3</sub> concentration in METHNx10 increased up to 6.9 ppb at Ouray and a greater amount at the coalbed methane gas field; total O<sub>3</sub> column concentrations increase up to 24 ppb (Figure 5.5). HO<sub>x</sub> and HCHO concentrations in METHNx10 increase by 36% and 23% respectively on average over REF.

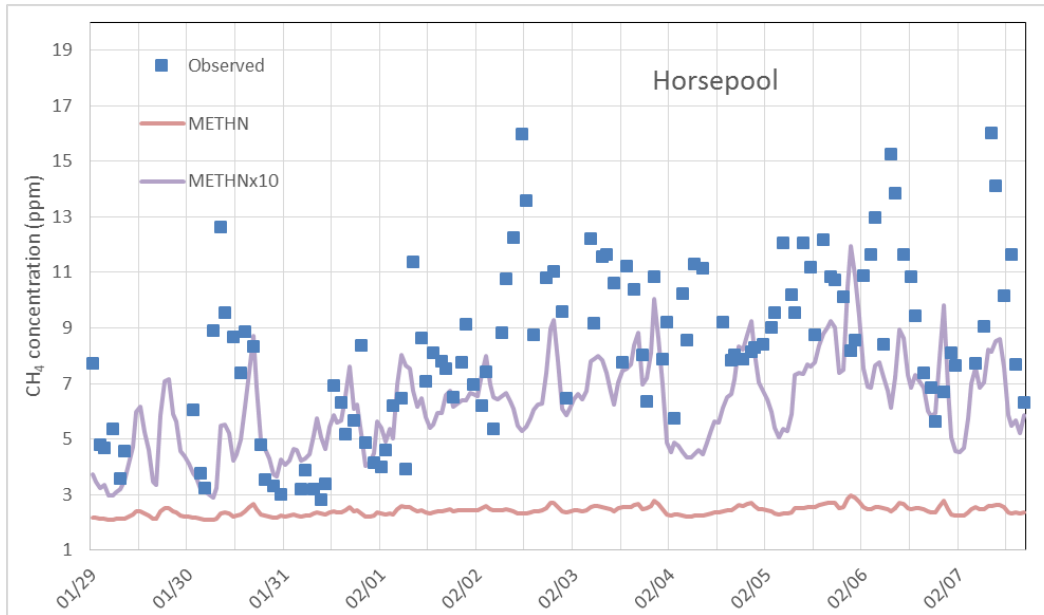


**Figure 5.4.** Comparison of observed to estimated CH<sub>4</sub> concentrations as simulated with “as-is” EI (METHN) and with CH<sub>4</sub> emissions arbitrarily increased 10 times (METHNx10) at Horsepool monitoring site.

CH<sub>4</sub> chemistry should have insignificant impact on O<sub>3</sub> formation under summer than winter conditions due to the abundance of water vapor during summer. To verify this hypothesis, we performed a REF and METHNx10 sensitivity simulations for a short episode of June 25-27, 2012 with CH<sub>4</sub> emission increased by 10 times. During this time, simulated water vapor mixing ratios at the surface in the Uintah Basin are up to  $7 \times 10^3$  ppm (compared to  $2 \times 10^3$  ppm in February 2013). At Horsepool, simulated CH<sub>4</sub> concentrations are up to 3 ppm and the O<sub>3</sub> concentrations only increase up to 0.25 ppb in METHNx10 over REF. This finding strengthens the important of CH<sub>4</sub> chemistry on O<sub>3</sub> formation under winter condition.

Based on this sensitivity study, we conclude that CH<sub>4</sub> chemistry is important for O<sub>3</sub> formation in the oil and gas field where CH<sub>4</sub> emissions are high and during wintertime when there is less water vapor in the atmosphere. Thus, photochemical model applications for winter O<sub>3</sub> studies should consider CH<sub>4</sub> chemistry in their chemical mechanisms. Our sensitivity study also showed that CH<sub>4</sub> emissions are probably underestimated by a large factor, and thus improvements in the EI are needed. Accurate estimations of CH<sub>4</sub> emission are not only important for photochemical model applications but also for greenhouse gas studies.

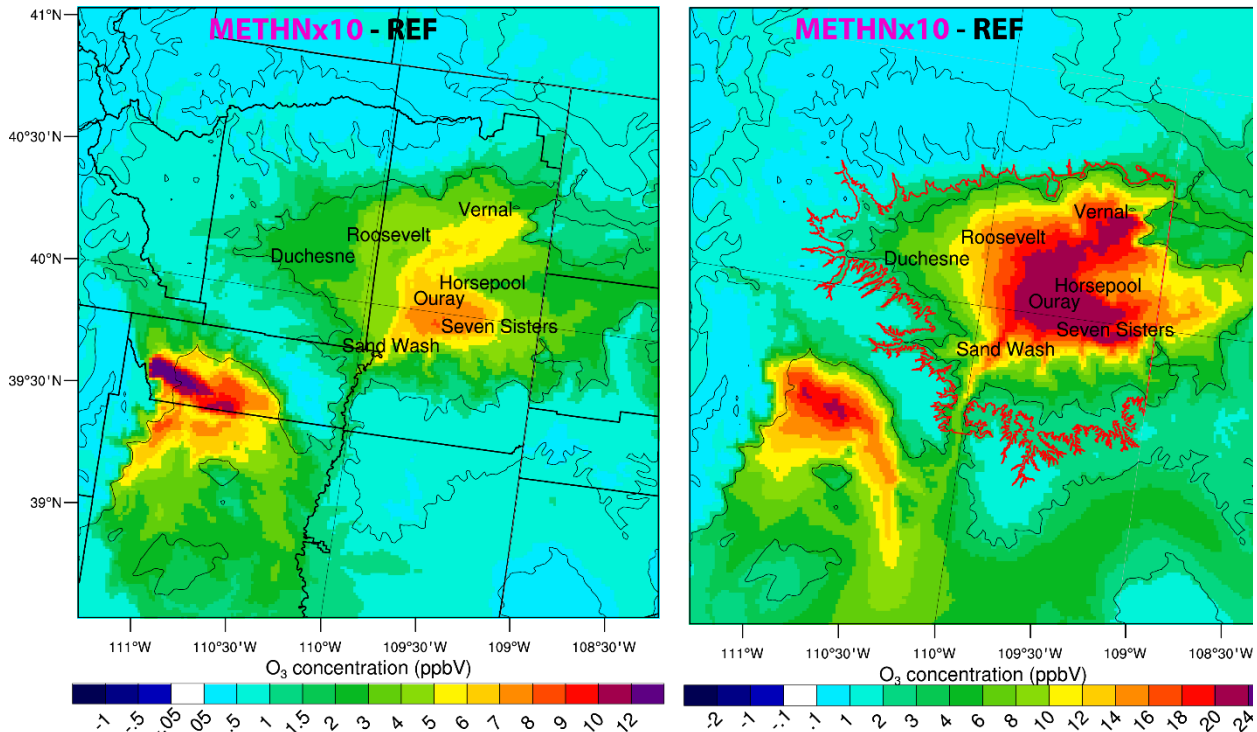


Figure 5.5. Analogous to Figure 5.1 but for METHNx10 – REF O<sub>3</sub>-differences.

### 5.3. Combination effects

Including all modifications to the SAPRC07 mechanism in the ALL simulation decreases surface O<sub>3</sub> concentration by 1.3 ppb on average over all monitoring sites in the Uintah Basin and by up to 5.4 ppb at Ouray. Reduction in total O<sub>3</sub> column-concentration in ALL is as high as 27 ppb. Reductions in O<sub>3</sub> concentration occur everywhere including the coalbed methane fields in Carbon and Emery counties and have their highest extent in the Uintah Basin (Figure 5.6).

In comparison with REF, HO<sub>x</sub> concentrations in ALL are higher during daytime but are lower during nighttime (by 10% on average). HCHO concentrations are higher in ALL than in REF during both day and nighttime (by 5.3 %). The inclusion of CH<sub>4</sub> chemistry in ALL partially contributed to the HCHO-differences between ALL and REF.

The net decrease in O<sub>3</sub> formation in ALL simulations is due to the updates in non-photolysis reactions to SAPRC07. For example, reaction <24> has been updated from negative-temperature-dependence (i.e., *k* increases as temperature decreases) to positive-temperature-dependence. The effects of the update to reaction <24> are that under low temperature less NO<sub>2</sub> was produced from reaction <24> while more NO was produced from HONO photolysis reaction which together led to reduction in O<sub>3</sub> formation. However, the net decrease in O<sub>3</sub> concentration in ALL should not be solely caused by updates to reaction <24> but rather by the combination of all updates to SAPRC07 mechanism. Evaluation of the impacts of these updates on O<sub>3</sub> require more comprehensive sensitivity simulations which are not in the scope of this study.

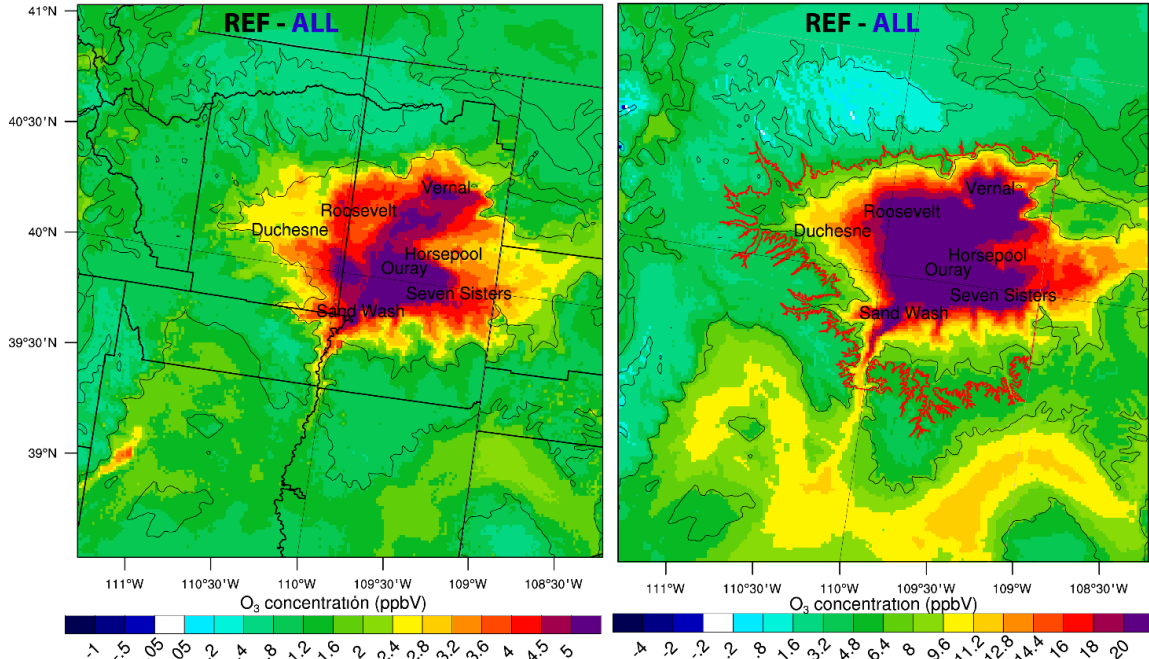


Figure 5.6. Analogous to Figure 5.1 but for REF - ALL O<sub>3</sub>-differences.

Figure 5.7 and Table 5.1 compare simulated O<sub>3</sub> concentrations estimated by all sensitivity simulations at several monitoring sites.

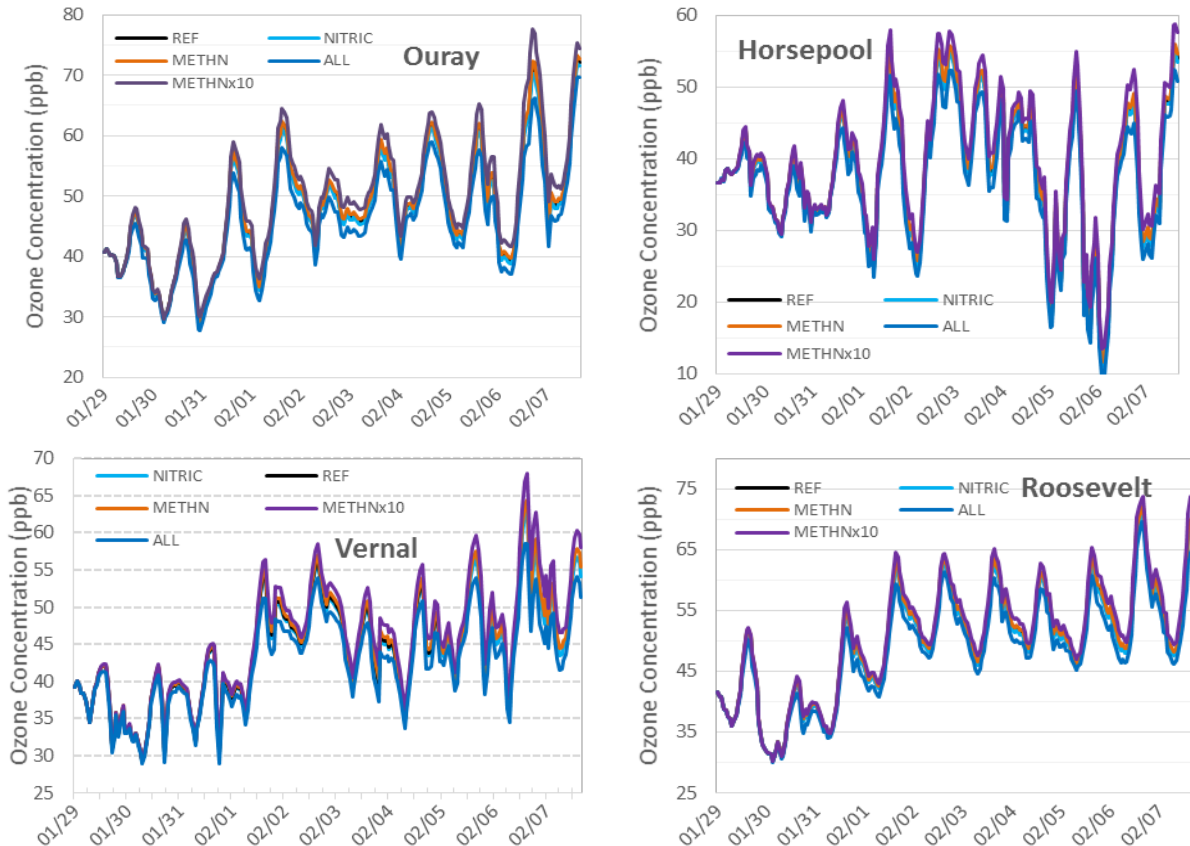


Figure 5.7. Comparison of simulated O<sub>3</sub> concentrations at four monitoring sites as obtained from REF, NITRIC, METHN, METHNx10 and ALL sensitivity simulations.

**Table 5.1.** Comparison of simulated O<sub>3</sub> concentrations at several monitoring sites in the Uintah Basin.

Station	O <sub>3</sub> concentrations (ppb)	REF	NITRIC	METHN	METHNx10	ALL
Horsepool	Overall average	38.4	38.1	38.7	39.9	36.7
	Highest 1-hour	55.4	54.9	56.0	58.7	52.4
	Highest 8-hour	53.2	52.6	53.7	55.9	50.1
	Highest difference ( - REF)	--	<b>-0.60</b>	<b>0.76</b>	<b>4.35</b>	<b>-3.64</b>
Ouray	Overall average	47.5	47.2	47.9	49.4	45.4
	Highest 1-hour	72.6	72.0	73.2	77.7	69.7
	Highest 8-hour	67.0	66.2	68.0	72.7	62.3
	Highest difference ( - REF)	--	-0.96	1.07	6.86	-5.41
Seven Sister	Overall average	42.7	42.4	43.1	44.5	40.8
	Highest 1-hour	65.2	64.4	66.1	70.4	61.1
	Highest 8-hour	57.4	56.8	58.0	60.6	54.0
	Highest difference ( - REF)	--	<b>-0.86</b>	<b>1.01</b>	<b>6.69</b>	<b>-4.97</b>
Red Wash	Overall average	38.6	38.4	38.9	39.9	37.1
	Highest 1-hour	57.5	57.0	58.0	59.6	55.1
	Highest 8-hour	50.9	50.4	51.3	52.8	48.7
	Highest difference ( - REF)	--	<b>-0.49</b>	<b>0.66</b>	<b>3.35</b>	<b>-3.29</b>
Vernal	Overall average	44.2	43.9	44.5	45.5	42.3
	Highest 1-hour	63.6	62.8	64.5	68.0	58.6
	Highest 8-hour	58.6	57.9	59.4	62.7	54.0
	Highest difference ( - REF)	--	<b>-0.75</b>	<b>0.89</b>	<b>4.54</b>	<b>-5.02</b>
Roosevelt	Overall average	49.7	49.4	50.0	50.8	48.0
	Highest 1-hour	71.8	71.2	72.2	73.7	69.5
	Highest 8-hour	67.0	66.4	67.4	68.8	64.7
	Highest difference ( - REF)	--	<b>-0.80</b>	<b>0.87</b>	<b>4.67</b>	<b>-4.56</b>
Duschene	Overall average	47.4	47.2	47.6	50.0	46.5
	Highest 1-hour	68.4	67.8	68.8	70.2	66.3
	Highest 8-hour	59.5	59.1	59.8	60.5	57.9
	Highest difference ( - REF)	--	<b>-0.56</b>	<b>0.48</b>	<b>2.07</b>	<b>-2.54</b>

## 6. CONCLUSIONS AND RECOMMENDATIONS

In this study, we successfully updated the SAPRC07 chemical mechanism with the latest literature data of photolysis and non-photolysis reactions to improve the accuracy of photochemical model simulations. Among the updates made to SAPRC07 mechanism, the inclusion of HNO<sub>3</sub> branching effect and the CH<sub>4</sub> chemistry are two updates aimed at improving the accuracy of photochemical models in simulating O<sub>3</sub> under low temperature conditions during winter in the Uintah Basin.

Inclusion of the HNO<sub>3</sub> branching effect resulted in a relatively small reduction in O<sub>3</sub> concentrations (up to

0.96 ppb) and a marginal increase in  $\text{HNO}_3$  and nitrate-aerosol concentrations which are consistent with literature reviews. We did not find a clear negative-relationship between  $\text{HNO}_3$  formation and air temperature due to the photochemical activity of the chosen episode, and we recommend a longer simulation episode for studying this relationship. The effects of enhancing  $\text{HNO}_3$  formation as demonstrated in this study, together with the enhancement of alkyl nitrate as demonstrated by Lee et al. (2014) under low temperature should be considered in photochemical models as they are important for  $\text{O}_3$  as well as aerosol air quality modeling studies.

The most important finding in this study is the non-trivial role of  $\text{CH}_4$  chemistry on  $\text{O}_3$  formation in winter when the atmosphere is dry and in oil and gas fields such as the Uintah Basin where  $\text{CH}_4$  concentrations are high. The sensitivity simulation with the current EI highly underestimated  $\text{CH}_4$  concentrations (3 ppm simulated vs 20 ppm observed). Given such  $\text{CH}_4$  model performance, inclusion of  $\text{CH}_4$  chemistry to SAPRC07 mechanism increases  $\text{O}_3$  concentration by up to 1.6 ppb. When we arbitrarily increased  $\text{CH}_4$  emission by 10 times, the simulated  $\text{CH}_4$  approached 12 ppm which is still lower than observed  $\text{CH}_4$ . Such an increase in  $\text{CH}_4$  emission resulted in a significant increase in  $\text{O}_3$  concentration (up to 6.9 ppb in the Uintah Basin). We conclude that simulations with adequate accuracy in  $\text{CH}_4$  emissions would result in a greater impact on  $\text{O}_3$  formation.

Combination of all updates made to the SAPRC07 mechanism resulted in a net reduction in  $\text{O}_3$  concentration (up to 5.4 ppb in the Basin). We believe the updates made to SAPRC07 mechanism are necessary and improved SAPRC07's accuracy in characterizing atmospheric chemical processes.

This study only performed updates to the SAPRC07 mechanism. However, such updates are applicable to other chemical mechanisms such as CB05 or SAPRC99. Thus we strongly recommend the implementation of updates presented in this study to other chemical mechanisms. Sensitivity simulations to evaluate effects of the updates to different chemical mechanisms should also be performed.

Clearly the EI needs to be improved for better photochemical model performance for studying air quality in the Uintah Basin. These improvements of EI should also include more representative VOC speciation profiles for emissions from the oil and gas industry. We believe that simulations with an improved EI and with the updated SAPRC07 mechanism would show impacts on  $\text{O}_3$  formation different from those reported in this study. We recommend such simulations should be performed when an improved EI becomes available.

## 7. REFERENCES

---

- AECOM. *Utah Air Resource Management Strategy Modeling Project: Air Quality Performance Evaluation*; Prepared for Bureau of Land Management - Utah State Office; Salt Lake City, UT, 2014; p 371.
- Avey, L.; Pennell, C.; Harper, K. In *CMAQ Sensitivity to Uintah Basin Oil and Gas Emissions Inventory Updates*, Western Air Quality Modeling Workshop, Boulder, CO, Boulder, CO, 2015.
- Blasing, T. J., Recent Greenhouse Gas Concentrations. Carbon Dioxide Information Analysis Center (CDIAC), [http://cdiac.ornl.gov/pns/current\\_ghg.html](http://cdiac.ornl.gov/pns/current_ghg.html) (accessed August 2015). Latest update dated February 2014.
- Burkholder, J. B.; Talukdar, R. K.; Ravishankara, A. R.; Solomon, S., Temperature Dependence of the HNO<sub>3</sub> UV Absorption Cross Sections. *Journal of Geophysical Research* **1993**, *98* (D12), 12.
- Butkovskaya, N. I.; Kukui, A.; Pouvesle, N.; Le Bras, G., Formation of Nitric Acid in the Gas-Phase HO<sub>2</sub> + NO Reaction: Effects of Temperature and Water Vapor. *The Journal of Physical Chemistry A* **2005**, *109* (29), 6509-6520.
- Byun, D. W.; Schere, K. L., Review of the governing equations, computational algorithms, and other components of the Models-3 Community Multiscale Air Quality (CMAQ) Modeling System. *Appl. Mech. Rev.* **2006**, *59* (2), 27.
- Carter, W. P. L., Development of the SAPRC-07 chemical mechanism. *Atmospheric Environment* **2010**, *44* (40), 5324-5335.
- Carter, W. P. L., Development of an Improved Chemical Speciation Database for Processing Emissions of Volatile Organic Compounds for Air Quality Models. College of Engineering, Center for Environmental Research and Technology, <http://www.engr.ucr.edu/~carter/emitdb/>. Latest update dated August 19, 2015.
- Carter, W. P. L.; Seinfeld, J. H., Winter ozone formation and VOC incremental reactivities in the Upper Green River Basin of Wyoming. *Atmospheric Environment* **2012**, *50*, 255-266.
- Carter, W. P. L.; Heo, G., Development of revised SAPRC aromatics mechanisms. *Atmospheric Environment* **2013**, *77* (0), 404-414.
- Chance, K.; Kurucz, R. L., An improved high-resolution solar reference spectrum for Earth's atmosphere measurements in the ultraviolet, visible, and near infrared. *J. Quant. Spectrosc. Radiat. Transf.* **2010**, *111*, 1289-1295.
- Chen, F.; Dudhia, J., Coupling an Advanced Land Surface-Hydrology Model with the Penn State-NCAR MM5 Modeling System. Part I: Model Implementation and Sensitivity. *Monthly Weather Review* **2001**, *129* (4), 569-585.
- Coll, I.; Pinceloup, S.; Perros, P. E.; Laverdet, G.; Le Bras, G., 3D analysis of high ozone production rates observed during the ESCOMPTE campaign. *Atmospheric Research* **2005**, *74* (1-4), 477-505.
- Emery, C.; Yarwood, G. In *Improvements to the CAMx Photochemical Model for Winter Ozone*, Air Quality in Utah: Science for Solutions II, Vernal, UT 84078, Vernal, UT 84078, 2015.
- Goliff, W. S.; Stockwell, W. R.; Lawson, C. V., The regional atmospheric chemistry mechanism, version 2. *Atmospheric Environment* **2013**, *68* (0), 174-185.
- Helmig, D.; Ganzeveld, L.; Butler, T.; Oltmans, S. J., The role of ozone atmosphere-snow gas exchange on polar, boundary-layer tropospheric ozone - a review and sensitivity analysis. *Atmos. Chem. Phys.* **2007**, *7*

(1), 15-30.

Helmig, D.; Stephens, C.; Park, J.-H.; Hueber, J.; Boylan, P.; Evans, J. *Ozone Deposition Velocity During Snow-covered and Non-snow-covered Periods by Eddy Covariance*; Uintah Basin 2013 Winter Ozone Study - Final Report; Utah Department of Environmental Quality, UT, 2014.

Houyoux, M. R.; Vukovich, J. M. Updates to the Sparse Matrix Operator Kernel Emissions (SMOKE) Modeling System and Integration with Models-3 (1999). In *The Emission Inventory: Regional Strategies for the Future*, Air and Waste Management Association, Raleigh, NC, 1999.

Iacono, M. J.; Delamere, J. S.; Mlawer, E. J.; Shephard, M. W.; Clough, S. A.; Collins, W. D., Radiative forcing by long-lived greenhouse gases: Calculations with the AER radiative transfer models. *Journal of Geophysical Research: Atmospheres* **2008**, *113* (D13103), p 8.

IUPAC, Evaluated Kinetic Data. IUPAC Task Group on Atmospheric Chemical Kinetic Data Evaluation, <http://iupac.pole-ether.fr/index.html> (accessed July 2015). Latest update dated July 2015.

Janjić, Z. I., The Step-Mountain Eta Coordinate Model: Further Developments of the Convection, Viscous Sublayer, and Turbulence Closure Schemes. *Monthly Weather Review* **1994**, *122* (5), 927-945.

Kain, J. S., The Kain–Fritsch Convective Parameterization: An Update. *Journal of Applied Meteorology* **2004**, *43* (1), 170-181.

Kemball-Cook, S.; Jia, Y.; Emery, C.; Morris, R.; Wang, Z.; Tonnesen, G. *Alaska MM5 Modeling for the 2002 Annual Period to Support Visibility Modeling*; Prepared for the Western Regional Partnership, Denver, Colorado; 2005.

Kircher, C. C.; Sander, S. P., Kinetics and mechanism of hydroperoxo and hydroperoxo-d disproportionations. *The Journal of Physical Chemistry* **1984**, *88* (10), 2082-2091.

Lee, L.; Wooldridge, P. J.; Gilman, J. B.; Warneke, C.; de Gouw, J.; Cohen, R. C., Low temperatures enhance organic nitrate formation: evidence from observations in the 2012 Uintah Basin Winter Ozone Study. *Atmospheric Chemistry and Physics* **2014**, *14* (22), 12441-12454.

Mihele, C. M.; Mozurkewich, M.; Hastie, D. R., Radical loss in a chain reaction of CO and NO in the presence of water: Implications for the radical amplifier and atmospheric chemistry. *International Journal of Chemical Kinetics* **1999**, *31* (2), 145-152.

Neemann, E. M.; Crosman, E. T.; Horel, J. D.; Avey, L., Simulations of a cold-air pool associated with elevated wintertime ozone in the Uintah Basin, Utah. *Atmos. Chem. Phys.* **2015**, *15* (1), 135-151.

National Operational Hydrologic Remote Sensing Center (NOHRSC). 2004, Snow Data Assimilation System (SNODAS) Data Products at NSIDC, 30 September 2003 to present Boulder, Colorado USA: National Snow and Ice Data Center. <http://dx.doi.org/10.7265/N5TB14TC>

Reichert, L.; Andrés Hernández, M. D.; Stöbener, D.; Burkert, J.; Burrows, J. P., Investigation of the effect of water complexes in the determination of peroxy radical ambient concentrations: Implications for the atmosphere. *Journal of Geophysical Research: Atmospheres* **2003**, *108* (D1), ACH 4-1-ACH 4-16.

Sander, S. P.; Friedl, R. R.; Ravishankara, A. R.; Golden, D. M.; Kolb, C. E.; Kurylo, M. J.; Molina, M. J.; Moortgat, G. K.; Finlayson-Pitts, B. J.; Wine, P. H.; Huie, R. E.; Orkin, V. L., Chemical Kinetics and Photochemical Data for Use in Atmospheric Studies - Evaluation Number 15. *Jet Propulsion Laboratory Publication 06-2* **2006**, 523.

Sander, S. P.; Friedl, R. R.; Abbatt, J. P. D.; Barker, J. R.; Burkholder, J. B.; Golden, D. M.; Kolb, C. E.; Kurylo, M. J.; Moortgat, G. K.; Wine, P. H.; Huie, R. E.; Orkin, V. L., Chemical Kinetics and Photochemical Data for Use in Atmospheric Studies - Evaluation Number 17. *Jet Propulsion Laboratory Publication 10-6* **2011**, 684.

Schocker, A.; Uetake, M.; Kanno, N.; Koshi, M.; Tonokura, K., Kinetics and Rate Constants of the Reaction  $\text{CH}_2\text{OH} + \text{O}_2 \rightarrow \text{CH}_2\text{O} + \text{HO}_2$  in the Temperature Range of 236-600 K. *J. Phys. Chem. A* **2007**, *111*, 6.

Serdyuchenko, A.; Gorshelev, V.; Weber, M.; Chehade, W.; Burrows, J. P., High spectral resolution ozone absorption cross-sections &ndash; Part 2: Temperature dependence. *Atmos. Meas. Tech. Discuss.* **2013**, *6* (4), 6613-6643.

Skamarock, W. C.; Klemp, J. B.; Dudhia, J.; Gill, D. O.; Barker, D. M.; Duda, M. G.; Huang, X.; Wang, W.; Powers, J. G. *A Description of the Advance Research WRF Version 3*; NCAR Technical Note NCAR/TN-475+STR, NCAR, Boulder, CO, 2008; p 125.

Sun, D.-Z.; Lindzen, R. S., Distribution of Tropical Tropospheric Water Vapor. *Journal of the Atmospheric Sciences* **1993**, *50* (12), 1643-1660.

Tesche, T. W.; McNally, D. E.; Tremback, C. *Operational Evaluation of The MM5 Meteorological Model over The Continental United States: Protocol for Annual and Episodic Evaluation*; Prepared for Mr. Pat Dolwick U.S. EPA Office of Air Quality Planning and Standards; 2002.

Thompson, G.; Field, P. R.; Rasmussen, R. M.; Hall, W. D., Explicit Forecasts of Winter Precipitation Using an Improved Bulk Microphysics Scheme. Part II: Implementation of a New Snow Parameterization. *Monthly Weather Review* **2008**, *136* (12), 5095-5115.

Tran, T.; Tran, H. WRF-CAMx Process Analysis: Winter Ozone Pollution in Uintah Basin. In *Air and Waste Management Association 108th Annual Conference, Paper # 220*, Raleigh, NC, 2015.

Tran, T.; Tran, H.; Mansfield, M.; Lyman, S. WRF-CAMx Modeling Study of Winter Ozone in Uintah Basin - A Case Study of January 15-23 in 2013. In *AGU Fall meeting 2014 - Poster Presentation*, San Francisco, CA, 2014.

Voigt, S.; Orphal, J.; Burrows, J. P., The temperature and pressure dependence of the absorption cross-sections of  $\text{NO}_2$  in the 250–800 nm region measured by Fourier-transform spectroscopy. *Journal of Photochemistry and Photobiology A: Chemistry* **2002**, *149*, 7.

Wild, O.; Zhu, X.; Prather, M., Fast-J: Accurate Simulation of In- and Below-Cloud Photolysis in Tropospheric Chemical Models. *Journal of Atmospheric Chemistry* **2000**, *37* (3), 245-282.

Yarwood, G.; Rao, S.; Yocke, M.; Whitten, G. *Updates to the Carbon Bond Chemical Mechanism: CB05*; Final Report to the US EPA, RT-0400675, 2005; p 246.

Zhang, L.; Brook, J. R.; Vet, R., A revised parameterization for gaseous dry deposition in air-quality models. *Atmos. Chem. Phys.* **2003**, *3* (6), 2067-2082.